

Robot Guidance Controller

Ravi Tejwani¹, John Payne¹, Karl Velazquez¹, Paolo Bonato^{2,3}, and Harry Asada⁴

¹Electrical Engineering and Computer Science, Massachusetts Institute of Technology,
Cambridge, MA 02139

²Department of Physical Medicine, Harvard Medical School

³Spaulding Rehabilitation Hospital, Charlestown, MA 02129

⁴Mechanical Engineering, Massachusetts Institute of Technology, Cambridge, MA 02139

Abstract

When human instructors guide learners through motor tasks, they seamlessly coordinate physical touch with verbal explanations - a dance teacher positions a student's arms while describing the movement, a therapist supports a patient's limb while offering encouragement. In contrast, a robot applying physical forces without verbal context can feel invasive or unsettling to humans. We present a robot guidance controller that learns to coordinate physical and verbal guidance as human instructors naturally do. Our system adaptively balances these modalities based on real-time estimation of human compliance: when learners struggle, it provides firmer physical corrections with explicit instructions; as they improve, it transitions to lighter touch with encouraging phrases. Our method comprises three components: (1) an estimator that infers physical and verbal compliance from tracking errors, (2) an optimization method that dynamically allocates guidance between force and language, and (3) a force-to-language model that generates contextually appropriate utterances. User studies ($N=12$) demonstrate that adaptive coordination of guidance significantly outperforms single-modality guidance and fixed-combination baselines: up to 50% reduction in tracking error, 39% improvement in movement smoothness, and 27% faster task completion. While validated in rehabilitation therapy, our approach generalizes to any human-robot collaborative learning scenario.

1 Introduction

As a child learns to write the letter "A" for the first time, their mother holds the child's hand, verbally explaining 'draw a line up and above' while simultaneously providing gentle nudges to guide the motion. When the child deviates from the intended path, the mother increases corrective feedback through more explicit instructions and firmer nudges. Conversely, as the child begins to follow the correct path, the mother reduces physical as-

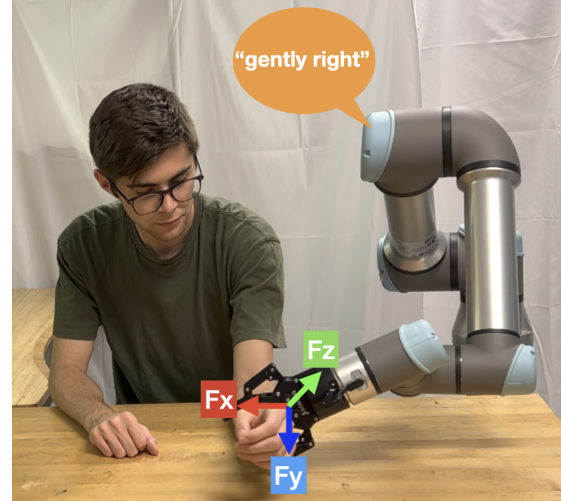


Figure 1: Our proposed method enables robots to guide humans through optimized verbal and physical guidance. It allows robots to estimate real time human compliance levels from their current state to generate appropriate guidance in the form of physical force corrections and instructional utterances. The method can be applied across various learning domains, adapting its guidance strategy based on universal principles of human guidance.

sistance and shifts to encouraging phrases such as 'you are going in the right direction', 'keep going', 'you got this'. This intuitive integration of verbal and physical guidance is ubiquitous in learning scenarios, from dance instruction and physical therapy to athletic training and vocational education (Figure 2).

Guidance is an intentional communication provided by an instructor to facilitate learning. It consists of two primary components: physical guidance in the form of force profiles (tactile forces applied to direct movement) and verbal guidance (instructional cues through speech).

In human-robot interaction, relying solely on physical guidance can be unsettling—direct force application from a robot may feel invasive or threatening to users

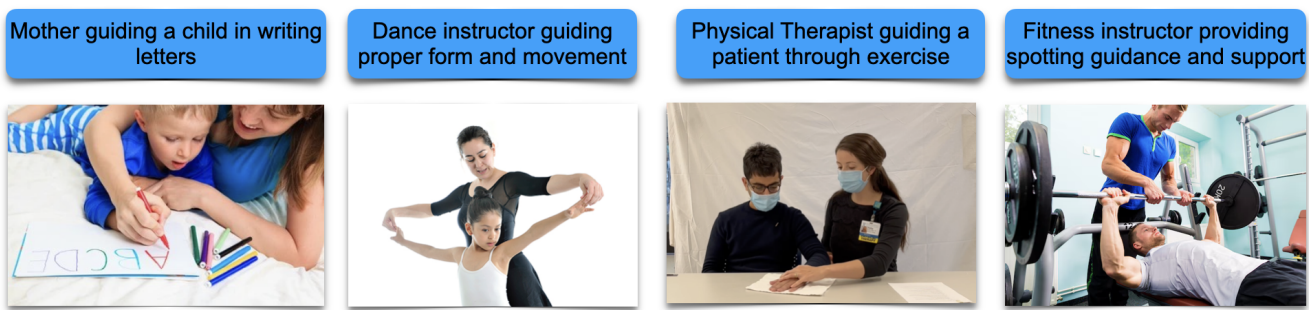


Figure 2: Integrated physical and verbal guidance across learning scenarios. From left to right: (1) A mother guides a child to write letters using coordinated guidance of hand gestures and verbal instructions; (2) A dance instructor combines physical positioning and verbal cues to guide proper form; (3) A physical therapist guides a patient through a rehabilitation exercise with adjustable physical support and encouraging feedback; (4) A fitness instructor provides spotting assistance and verbal coaching during weight training. In each scenario, the instructor dynamically balances physical and verbal guidance based on the learner’s needs—applying greater force and more explicit instructions when the learner deviates from the desired path, and transitioning to lighter guidance with encouraging feedback as performance improves.

[7, 16]. Verbal guidance serves as a crucial complement, providing cognitive context that helps users understand and anticipate the robot’s actions. This dual-modality approach not only improves task performance but also enhances user comfort and trust in the robotic system.

Language and force profiles are fundamentally heterogeneous, presenting significant integration challenges. Force can be applied continuously with precisely controlled magnitude and direction across X, Y, and Z axes for specific durations, creating immediate spatial corrections. Language, in contrast, comprises discrete words and phrases with semantic content that requires interpretation by the learner. While force provides quantitatively measurable feedback, language conveys abstract concepts that must be processed within the learner’s cognitive framework. This inherent heterogeneity necessitates an approach where verbal and physical guidance must be optimally computed and delivered in synchronization to the learner based on their evolving needs and compliance levels.

Across diverse learning scenarios (Figure 2), several critical questions emerge regarding the instructor’s decision-making process:

- What words to speak and when to speak? (Verbal Guidance)
- How much force to apply, in which direction, and for what duration? (Physical Guidance)
- How to adapt these decisions based on the learner’s changing behavioral states/compliance levels? (Optimization)

Our research objective is to encode these adaptive guidance capabilities within a robotic system (Figure 1) that

can effectively guide human learners with the same coordinated physical and verbal guidance provided by human instructors.

We propose a Robot Guidance Controller that enables a robot to optimally deliver physical and verbal guidance based on the learner’s estimated compliance states. The controller integrates three components: (1) a compliance estimator that infers physical and verbal compliance levels from observable behavior, such as position and velocity errors; (2) an optimization method that computes optimal physical force (magnitude, direction, and duration) and verbal instructions (contextually appropriate words) based on the inferred compliance states in real time; and (3) a force-to-language model that generates contextually appropriate utterances.

Research in robot guidance capabilities has been explored on topics such as teaching by demonstration [2], programming by demonstration [14, 15], skill acquisition [1, 13], and imitation learning [21, 10, 18]. These methods focus primarily on how robots can acquire and reproduce skills, ignoring the adaptive guidance aspect of instruction. When robots were deployed in interactive scenarios with humans, they typically either provided purely verbal instructions without physical guidance, or offered physical assistance without adaptive verbal feedback. Furthermore, existing systems that incorporated both modalities [5, 8, 20, 4] typically used pre-programmed fixed strategies [6, 25, 9, 11]. Our Robot Guidance Controller enables robots to provide coordinated and optimal physical and verbal guidance that continuously adapts to the human’s compliance states [26, 12, 24].

Our proposed method is fundamentally task-agnostic—designed to generalize across diverse learning scenarios from writing and dance to rehabilitation and

athletics (Figure 2). The controller is underpinned by universal principles of how instructors deliver and adapt guidance to learners. To demonstrate this generalizability, we derived insights from one representative instructor-learner interaction: physical therapists guiding patients during therapeutic exercises. We conducted an observational study at Spaulding Rehabilitation Hospital, analyzing interactions between therapists and patients during shoulder flexion exercises. This study revealed how expert instructors dynamically balance physical correction and verbal feedback based on the patient’s compliance levels—increasing assistive forces when encountering resistance and transitioning from instructional to encouraging language as performance improves (Figure 3). While our empirical validation focuses on this rehabilitation context, the controller’s design principles apply broadly across learning scenarios [17, 3, 22].

We make the following contributions:

1. A formalized framework for coordinating physical and verbal guidance in human-robot interaction
2. An adaptive optimization approach that distributes guidance across physical force and verbal instructions according to estimated compliance levels
3. A state estimation method for inferring human compliance levels from observable behaviors
4. Experimental validation through user studies demonstrating the controller’s effectiveness over baselines

2 Results

2.1 Study Procedure

The user study included 12 participants (8 males, 4 females) with a mean age of 23 years. The study procedures and protocol were reviewed and approved by the Institutional Review Board (IRB Protocol #2212000845R001), ensuring we followed ethical guidelines for human subject research. The UR5 robot guided users through a predefined reference trajectory. Participants sat beside the robot and placed their hand on the desk.

2.2 Study Design

We conducted two separate studies with each participant to evaluate different guidance methods provided by the robot.

Study 1: Comparison of Guidance Modalities. We had each user interact with each of the following

¹Online Appendix showcasing the video demonstrations and results for all the users https://robot-guidance-controller.github.io/user_study/.

guidance methods through multiple trials. In each trial, they were asked to exhibit a specific compliance behavioral state.

- **Verbal Guidance Only:** Vision-based tracking system that monitored hand position via camera and provided spoken directional cues when users deviated from the reference trajectory.
- **Physical Guidance Only:** Robot applied corrective forces using a PD (Proportional-Derivative) controller along the axis of deviation, guiding users back to the reference path without verbal feedback.
- **Combined Verbal and Physical Guidance:** A baseline robot controller that simultaneously delivers physical forces and verbal instructions to guide the user. This approach does not estimate user compliance. It provides dual guidance solely on the user’s position and velocity deviations from the reference trajectory.

Study 2: Robot Controller Comparison. This study evaluated our proposed method (Robot Guidance Controller), which *optimally* allocates physical and verbal guidance based on real-time user *compliance estimation* (Section 4). We compared our method to the baseline method from Study 1.

2.3 Research Questions

We investigated two main research questions:

1. Does combined verbal and physical guidance outperform single-modality guidance (physical-only or verbal-only)?
2. Does the Robot Guidance Controller method, which provides optimal adaptive guidance by tracking user state, outperform the baseline robot controller method?

2.4 Evaluation Metrics

We evaluated our methods using the following metrics:

- **Position Error:** Mean absolute error (MAE) between the user’s actual position and the reference position, calculated as $\text{MAE} = \frac{1}{N} \sum_{i=1}^N \|x_i - x_{ref,i}\|$, where x_i is the user’s position at time i .
- **Velocity Error:** MAE between the user’s velocity and the reference velocity, computed as $\text{MAE}_v = \frac{1}{N} \sum_{i=1}^N \|\dot{x}_i - \dot{x}_{ref,i}\|$, capturing the temporal accuracy of movement execution.
- **Movement Smoothness:** Quantified using the standard deviation of the velocity magnitude over time. Calculated as: $S =$

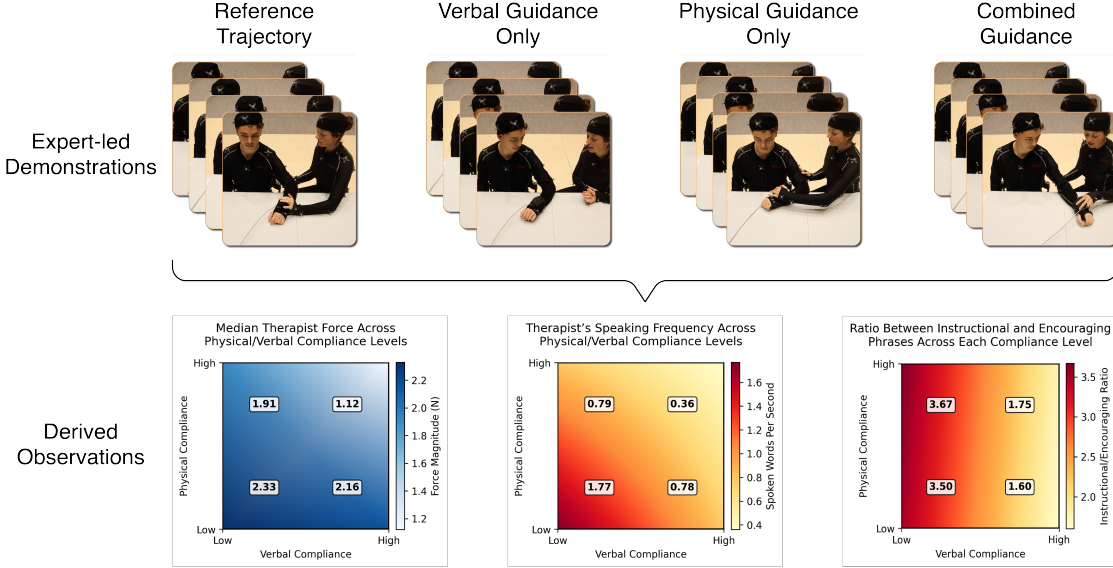


Figure 3: Observational study design and key findings from expert-led demonstrations. Top row: Four experimental conditions used to isolate guidance modalities—reference trajectory (passive patient), verbal-only, physical-only, and combined guidance. Bottom row: Analysis reveals adaptive guidance patterns across compliance states. (a) Median physical force decreases as verbal and physical compliance together progressively increase. (b) Speaking frequency reduces from 1.77 to 0.36 words/second with higher verbal compliance. (c) Language content shifts from instructional (ratio 3.67) to encouraging (ratio 1.60) as verbal compliance improves. These patterns demonstrate how expert instructors naturally adapt both the intensity and nature of guidance based on learner compliance levels. Full experimental details and analysis in Appendix A.

$\sqrt{\frac{1}{N-1} \sum_{i=1}^N (\|\dot{x}_i\| - \mu_v)^2}$, where μ_v is the mean velocity magnitude. Lower values indicate smoother motion.

- **Time to Completion:** Total time required to complete the task.
- **Frequency of Words Spoken:** Average number of words per second spoken during task execution, indicating the intensity of verbal guidance provided.
- **Ratio of Instructional to Encouraging Phrases:** Ratio of instructional phrases (e.g., “move left”, “push harder”) to encouraging phrases (e.g., “good job”, “keep going”), calculated by classifying each utterance and computing the ratio $R = N_{inst}/N_{enc}$.

2.5 Observational Data from Expert-Led Demonstrations

To understand how instructors naturally provide adaptive guidance, we collected observational data from the Chief Physical Therapist guiding patients during shoulder rehabilitation exercises at Spaulding Rehabilitation Hospital (Figure 3). Detailed analysis is in Appendix A).

The analysis revealed two key adaptive patterns. Physical guidance varied inversely with patient compli-

ance—therapists applied stronger corrective forces when patients exhibited low compliance and reduced intervention as physical compliance improved. Verbal guidance showed similar adaptation through both frequency and content. When verbal compliance was low, therapists spoke more frequently using instructional language. As verbal compliance increased, the frequency of speaking decreased, and the language shifted from instructional to encouraging phrases.

These patterns showed that effective guidance naturally adapts to learner state, reducing both physical intervention and instructional explicitness as compliance improves. This motivated the robot guidance controller.

2.6 Experimental Results

2.6.1 Research Question 1

To determine whether combining verbal and physical modalities yields improved task performance, we compared each single-modality with a combined-modality controller baseline in which the user’s compliance levels were varied. Deep dive analysis of a user for each of the modality is presented in Figure 4 5 6 and quantified in Table 1. Results and analysis of all the 12 users can be found in our Online Appendix¹

¹Online Appendix showcasing the video demonstrations and results for all 12 users: https://robot-guidance-controller.github.io/user_study/.

Deep Dive Analysis of a User with Baseline Method (Verbal Guidance Only)

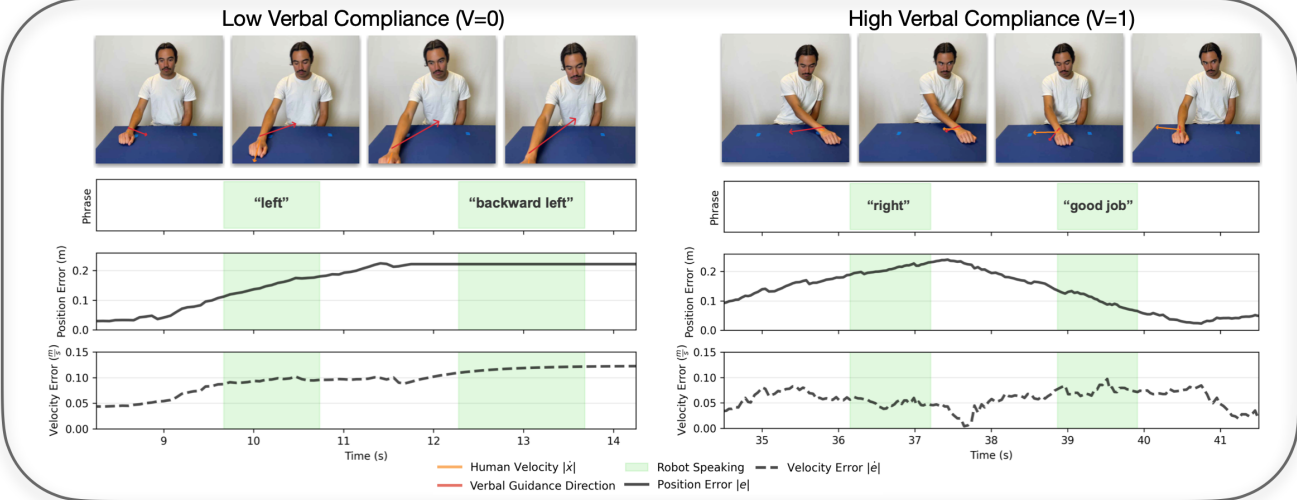


Figure 4: Representative trials under the “verbal guidance only” condition, contrasting low (left) versus high (right) verbal compliance. Top row: still frames sampled at equal time intervals. Second row: timeline of phrases; green shading denotes the periods when the robot is speaking. Third and fourth rows: evolution of task-space errors. The solid black trace is the position error $\|e\|$, the dashed trace is the velocity error $\|\dot{e}\|$, and the solid orange line is the user’s absolute hand speed $\|\dot{x}\|$. In the low-compliance example the participant largely ignores the commands, leading to monotonically rising errors. In the high-compliance case the same verbal cues prompt an immediate trajectory correction: position and velocity errors peak during the command “right” and drop sharply thereafter, illustrating the performance gain when speech is attended.

Low Verbal Compliance. Under low verbal compliance ($V = 0$), introducing physical guidance halved the position-tracking error even when participants were physically noncompliant ($P = 0, -52\%, p < 0.01$; Table 1a). When they were physically compliant ($P = 1$) the reduction deepened to 73% ($p < 10^{-4}$) and was accompanied by parallel gains in velocity error (−53%), smoothness (−73%) and a 43% cut in completion time.

High Verbal Compliance. Naturally high verbal compliance ($V = 1$) resulted in higher task accuracy when compared to low verbal compliance, however adding physical guidance managed to improve performance even further (Table 1b). Position error fell by 47% ($p < 10^{-3}$) under physical non-compliance ($P = 0$) and by 63% ($p < 10^{-4}$) under physical compliance ($P = 1$). Smoothness improved by 49–67%, and completion time shortened by nearly one-half when both channels were followed. Hence, physical cues remain valuable even when verbal instruction is well attended, with their impact depending on the degree of physical compliance.

Low Physical Compliance. When physical compliance was low ($P = 0$), speech was helpful only if users actively attended to it (Table 1c). Under verbal noncompliance ($V = 0$), verbal guidance produced no change in any metric, whereas active listening ($V = 1$) reduced position and velocity errors by 29% and 41%, respectively, and improved smoothness by 23% (all $p < 0.01$). Task completion time decreased (−8%, $p = 0.33$).

High Physical Compliance. In contrast, when physical guidance was already adhered to ($P = 1$) verbal augmentation yielded no statistically significant benefit (Table 1d). None of the accuracy or kinematic indices changed ($p > 0.14$), and unheeded speech ($V = 0$) actually prolonged task time by 52% ($p \approx 1$). These findings indicate that once the physical channel approaches ceiling performance, additional verbal content provides little incremental value.

Consensus. Overall, combining both verbal and physical modalities yields improved task performance when compared to single-modality guidance. The user scenarios are summarized graphically in Figure 7 and quantified in Table 1. We observed that introducing a second guidance modality improved task performance. The most pronounced gains—up to a 73% drop in position error, a 67% increase in smoothness, and a 48% reduction in completion time—appeared when the newly added modality was introduced while the original modality was ignored. When compliance with both modalities was already high, incremental benefits diminished, indicating a ceiling effect.

2.6.2 Research Question 2

To further investigate whether adapting and providing optimal physical vs. verbal guidance based on users compliance levels yields further benefit beyond simply deliv-

Deep Dive Analysis of a User with Baseline Method (Physical Guidance Only)

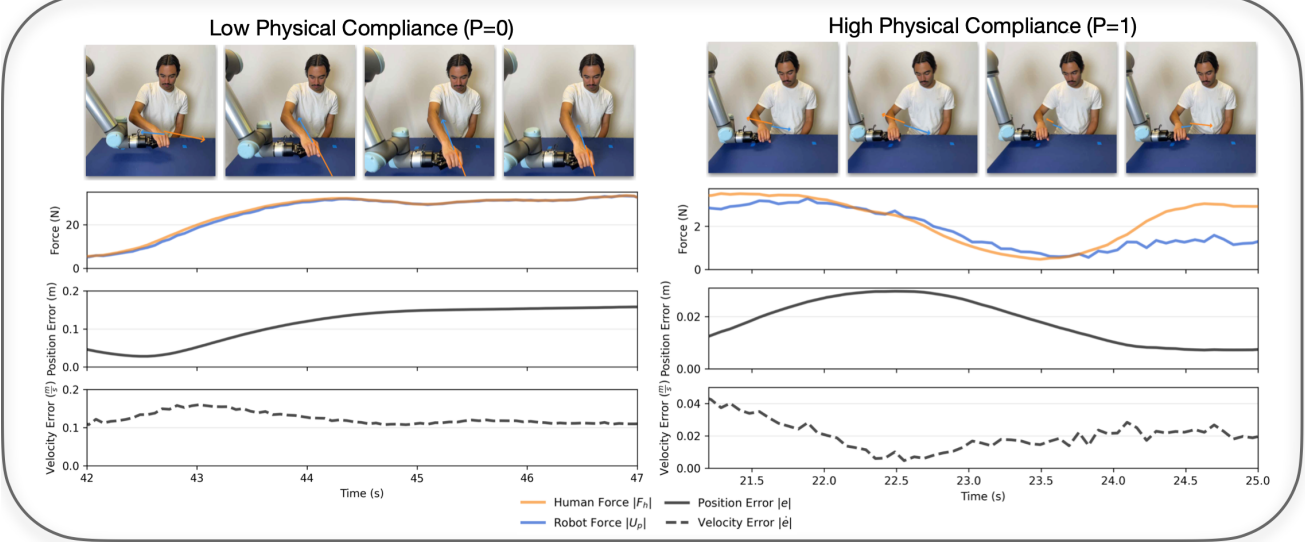


Figure 5: Representative trials under the “physical guidance only” condition, contrasting low (left column) versus high (right column) physical compliance. Top row: equally spaced video frames; arrows show the direction of the robot-applied force. Second row: interaction forces—orange is the magnitude of the human’s counter-force $\|F_h\|$, blue is the robot’s applied force $\|U_p\|$. Third and fourth rows: evolution of task-space errors. The solid black trace is position error $\|e\|$; the dashed black trace is velocity error $\|\dot{e}\|$. In the low-compliance example the participant resists the robot’s push; both forces climb in tandem but position and velocity errors continue to grow, indicating limited corrective benefit. In the high-compliance example the participant yields almost immediately: robot and human forces taper off, and both error signals decline.

ering both at once, we compared the fixed-gain “Baseline” controller used in Section 2.6.1 with our proposed robot guidance controller (“Our Method”). Visualizations of our results are provided in Figures 9-10 and numerical values of our results are provided in Appendix Table 2. Deep dive analysis of a user is presented in Figure 8. Results and analysis of all the 12 users can be found in our Online Appendix¹

Low verbal and physical compliance. When participants followed neither force nor speech, our controller reduced the position-tracking error by half (-50% , $p = 0.002$) as well as the movement smoothness (-50% , $p < 10^{-4}$), and reducing completion time by 27% ($p = 0.038$). Although the normalized median robot force did not move statistically ($p = 0.34$), our method spoke more often ($+26\%$, $p = 0.004$) and shifted its utterance mix from an instruction-heavy 2.31 toward the therapist’s 1.33 instruction-to-encouragement ratio (1.20, $p = 0.038$), demonstrating closer linguistic alignment with expert practice.

Physical compliance only. With force cues obeyed but speech ignored, our controller delivered a 48% drop in position error ($p = 0.009$) and a 39% gain in smoothness ($p = 0.011$) while maintaining task duration. Normalized robot force was further below the observational median than the baseline (0.57 vs. 0.79, $p = 0.79$),

yet speaking frequency nearly matched the therapist rate (0.87 w/s vs. 0.85 w/s) and the instruction-to-encouragement ratio moved decisively toward the target (0.96 vs. 1.40).

Verbal compliance only. When participants listened but resisted force, our adaptive controller still lowered position error by 29% ($p = 0.039$) and smoothness by 30% ($p = 0.043$); velocity error and time showed no reliable change. Notably, the controller demonstrated an increase in its normalized median force to 1.14, almost perfectly matching the therapist median (1.15) whereas the baseline remained lower (0.88). Its speech, however, became slightly more verbose and instructional than the expert, leaving baseline closer on those two linguistic metrics.

Full compliance. When the human fully adhered to both force cues and verbal instructions, performance saturated: none of the kinematic differences reached significance (all $p > 0.21$). Our controller spoke substantially less than the baseline (-23% , $p < 10^{-4}$) and produced an instruction-to-encouragement balance (0.72) much nearer the therapist’s (0.67) than the baseline did (0.43). The smaller robot force (0.48) diverged from the therapist level (0.60), suggesting force adaptation remains conservative under ceiling performance.

Deep Dive Analysis of a User with Baseline Method (Physical + Verbal Guidance)

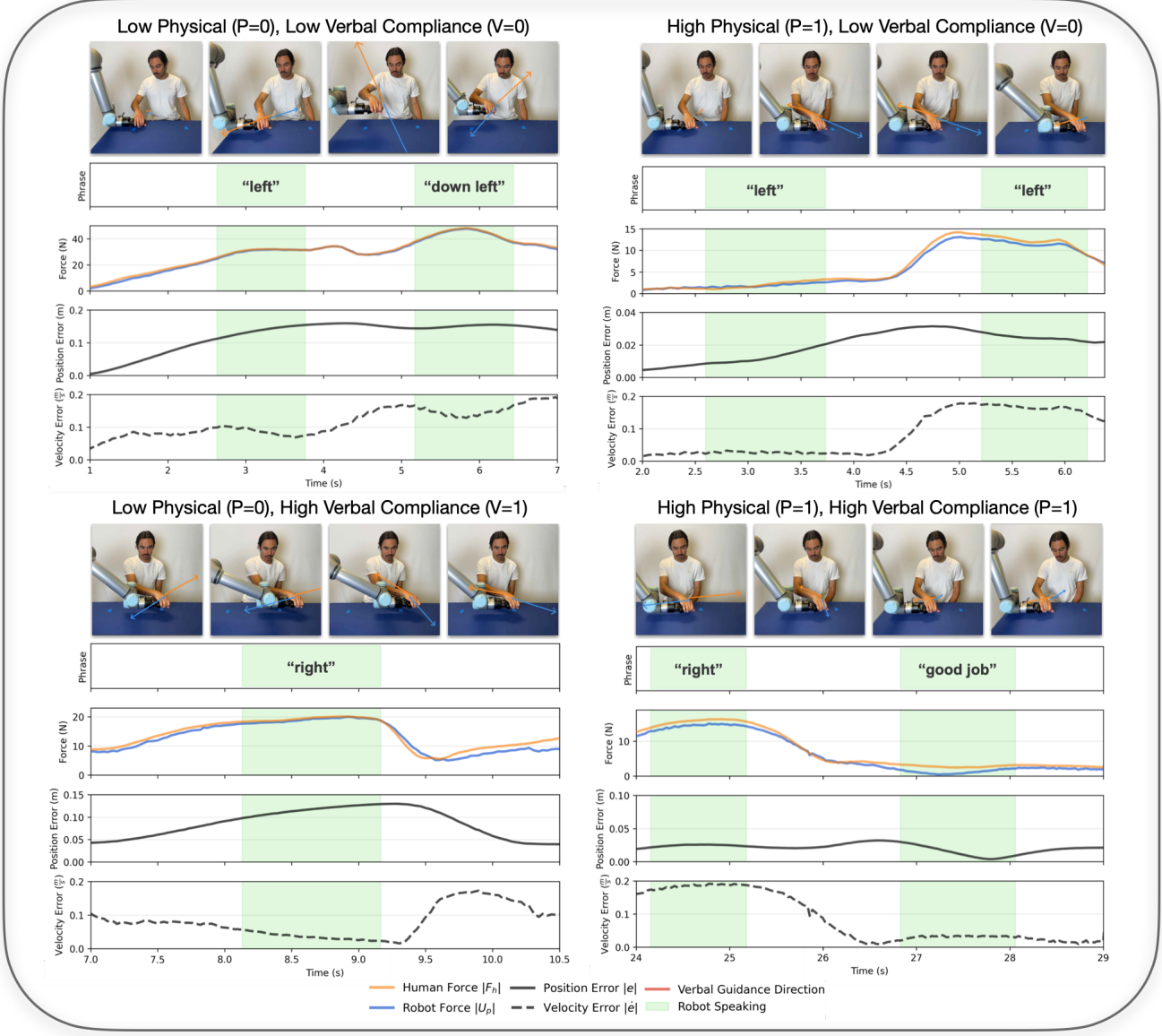


Figure 6: Each quadrant shows a single participant run when both physical and verbal channels were enabled, but the learner’s willingness to follow each channel differed: (a) low physical, low verbal; (b) high physical, low verbal; (c) low physical, high verbal; (d) high physical, high verbal. Top strip of each panel: equally spaced video frames with orange arrows depicting the direction requested by the robot’s spoken cue. Row 2: timeline of utterances; green shading marks robot-speaking intervals. Row 3: interaction forces (orange = human force $\|F_h\|$, blue = robot force $\|U_p\|$). Rows 4-5: task-space errors (solid black = position error $\|e\|$, dashed black = velocity error $\|ė\|$). The examples demonstrate how performance depends on channel compliance. When both channels are ignored (a), large forces build and errors grow despite repeated commands. When only the physical channel is heeded (b), forces translate quickly into error reduction even though words are ignored. The converse holds in (c): compliant listening lets the robot keep forces low while errors fall after the utterance “right.” Finally, with full compliance (d) the robot scarcely has to intervene: both forces decay and errors remain minimal, demonstrating efficient collaboration when the learner attends to both force and speech.

Consensus. Our robot guidance controller delivers significant improvements when compared to baseline controller in position and velocity accuracy (13–50%), smoothness (8–50%) and completion time (down by

27%). We observed that our robot controller reproduces expert speech patterns more closely than the fixed baseline—particularly in speaking frequency and directive balance—while its force magnitude still trails therapist

(a) Effect of adding *physical* guidance under **low verbal compliance** ($V=0$).

Metric	Verbal Guidance Only	+ Physical Guidance ($P = 0$)			+ Physical Guidance ($P = 1$)		
		Value	$\Delta\%$	p-value	Value	$\Delta\%$	p-value
Position Error (m)	0.120 ± 0.030	0.058 ± 0.016	$\downarrow \mathbf{52}$	0.0021^{**}	0.033 ± 0.012	$\downarrow \mathbf{73}$	0.00014^{***}
Velocity Error (m/s)	0.083 ± 0.010	0.069 ± 0.010	$\downarrow 17$	0.086	0.039 ± 0.010	$\downarrow \mathbf{53}$	0.00014^{***}
Smoothness (m/s)	0.067 ± 0.009	0.030 ± 0.005	$\downarrow \mathbf{55}$	$8.4 \times 10^{-6}^{***}$	0.018 ± 0.004	$\downarrow \mathbf{73}$	$2.2 \times 10^{-6}^{***}$
Completion Time (s)	120.6 ± 43.1	93.7 ± 25.0	$\downarrow \mathbf{22}$	0.0426^*	69.0 ± 12.3	$\downarrow \mathbf{43}$	0.0280^*

(b) Effect of adding *physical* guidance under **high verbal compliance** ($V=1$).

Metric	Verbal Guidance Only	+ Physical Guidance ($P = 0$)			+ Physical Guidance ($P = 1$)		
		Value	$\Delta\%$	p-value	Value	$\Delta\%$	p-value
Position Error (m)	0.064 ± 0.008	0.034 ± 0.009	$\downarrow \mathbf{47}$	0.00062^{***}	0.024 ± 0.010	$\downarrow \mathbf{63}$	0.000064^{***}
Velocity Error (m/s)	0.068 ± 0.013	0.040 ± 0.009	$\downarrow \mathbf{41}$	0.0036^{**}	0.030 ± 0.005	$\downarrow \mathbf{56}$	0.00020^{***}
Smoothness (m/s)	0.039 ± 0.007	0.020 ± 0.005	$\downarrow \mathbf{49}$	0.00030^{***}	0.013 ± 0.004	$\downarrow \mathbf{67}$	$1.1 \times 10^{-5}^{***}$
Completion Time (s)	86.9 ± 28.8	67.7 ± 15.9	$\downarrow 22$	0.138	45.4 ± 4.2	$\downarrow \mathbf{48}$	0.0113^*

(c) Effect of adding *verbal* guidance under **low physical compliance** ($P=0$).

Metric	Physical Guidance Only	+ Verbal Guidance ($V = 0$)			+ Verbal Guidance ($V = 1$)		
		Value	$\Delta\%$	p-value	Value	$\Delta\%$	p-value
Position Error (m)	0.048 ± 0.015	0.058 ± 0.016	$\uparrow 21$	0.947	0.034 ± 0.009	$\downarrow \mathbf{29}$	0.0387^*
Velocity Error (m/s)	0.068 ± 0.013	0.069 ± 0.010	$\uparrow 1$	0.619	0.040 ± 0.009	$\downarrow \mathbf{41}$	0.00018^{***}
Smoothness (m/s)	0.026 ± 0.006	0.030 ± 0.005	$\uparrow 15$	0.905	0.020 ± 0.005	$\downarrow \mathbf{23}$	0.0077^{**}
Completion Time (s)	73.5 ± 13.2	93.7 ± 25.0	$\uparrow 27$	0.930	67.7 ± 15.9	$\downarrow 8$	0.325

(d) Effect of adding *verbal* guidance under **high physical compliance** ($P=1$).

Metric	Physical Guidance Only	+ Verbal Guidance ($V = 0$)			+ Verbal Guidance ($V = 1$)		
		Value	$\Delta\%$	p-value	Value	$\Delta\%$	p-value
Position (m)	0.032 ± 0.013	0.033 ± 0.012	$\uparrow 3$	0.582	0.024 ± 0.010	$\downarrow 25$	0.069
Velocity (m/s)	0.027 ± 0.007	0.039 ± 0.010	$\uparrow 44$	0.998	0.030 ± 0.005	$\uparrow 11$	0.801
Smoothness (m/s)	0.015 ± 0.005	0.018 ± 0.004	$\uparrow 20$	0.848	0.013 ± 0.004	$\downarrow 13$	0.144
Completion Time (s)	45.4 ± 5.1	69.0 ± 12.3	$\uparrow 52$	0.999	45.4 ± 4.2	$\downarrow 0$	0.500

Table 1: Effect of adding the complementary guidance modality under each compliance regime. Numbers are the means plus or minus the 95% confidence interval; $\Delta\%$ is the relative change from the single-modality baseline. Two-tailed paired t -tests produce the p -values with significance markers ($*$ < 0.05 , $** < 0.01$, $*** < 0.001$). Boldface highlights the significant improvements ($p < 0.05$).

norms in two of the four compliance states. Overall, these results validate the premise that optimally weighting force and language yields better task performance and better emulates instructor teaching.

3 Discussion

While our Robot Guidance Controller demonstrates effective coordination of physical and verbal guidance, there remains certain limitations. Our Compliance estimator models compliance as binary states (high/low) for both physical and verbal dimensions. Although this simplification proved sufficient in the rehabilitation setting, human compliance is on a continuous range. Future work could extend the Bayesian filter to estimate continuous compliance values. We validated our method

on rehabilitation domain. While our method’s design principles are task-agnostic, extending to more complex movements such as multi-joint coordination tasks would require learning task-specific reference trajectories and potentially adjusting the PD gain parameters. Force-to-language mapping may also need expansion to accommodate a richer vocabulary for more diverse movement instructions. Despite these limitations, our results demonstrate that coordinated physical and verbal guidance significantly improves human-robot collaboration compared to single-modality approaches. These limitations primarily represent opportunities for extending the framework rather than fundamental constraints on the approach.

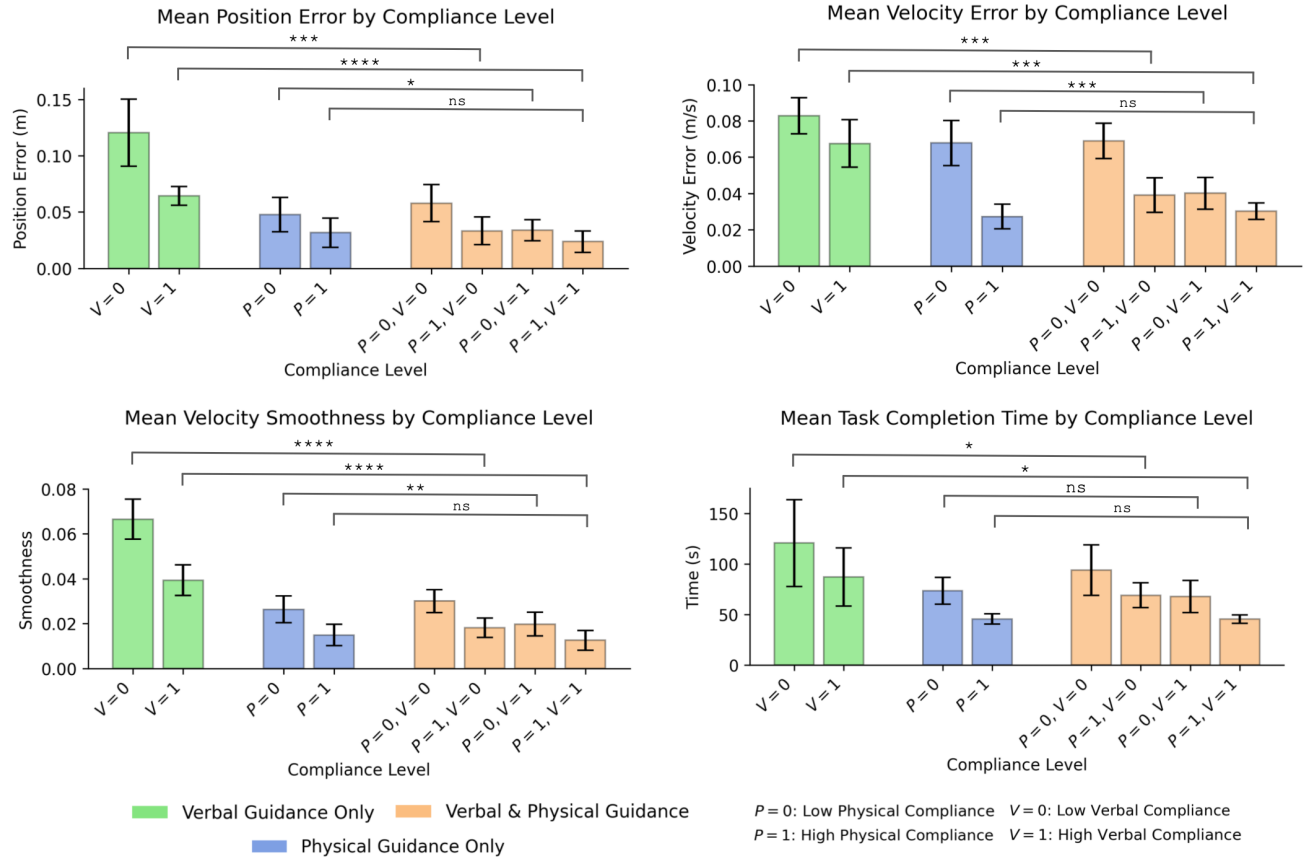


Figure 7: Performance of verbal-only (green), physical-only (blue), and combined guidance (orange) across varying compliance regimes. Each subplot shows a different evaluation metric: position error (top left), velocity error (top right), velocity smoothness (bottom left), and task completion time (bottom right). Bars are grouped by compliance level: single-modality levels (first and second clusters) and combined-modality levels under all four combinations of physical (P) and verbal (V) compliance (third cluster). Error bars indicate 95% confidence intervals. Statistically significant differences are marked with standard notation (* $p < 0.05$, ** $p < 0.01$, *** $p < 0.001$, **** $p < 0.0001$, ns = not significant). Results show that performance improves with compliance, and combining modalities helps most when one is ignored—allowing the other to compensate.

Deep Dive Analysis of a User with Robot Guidance Controller (Our Method)

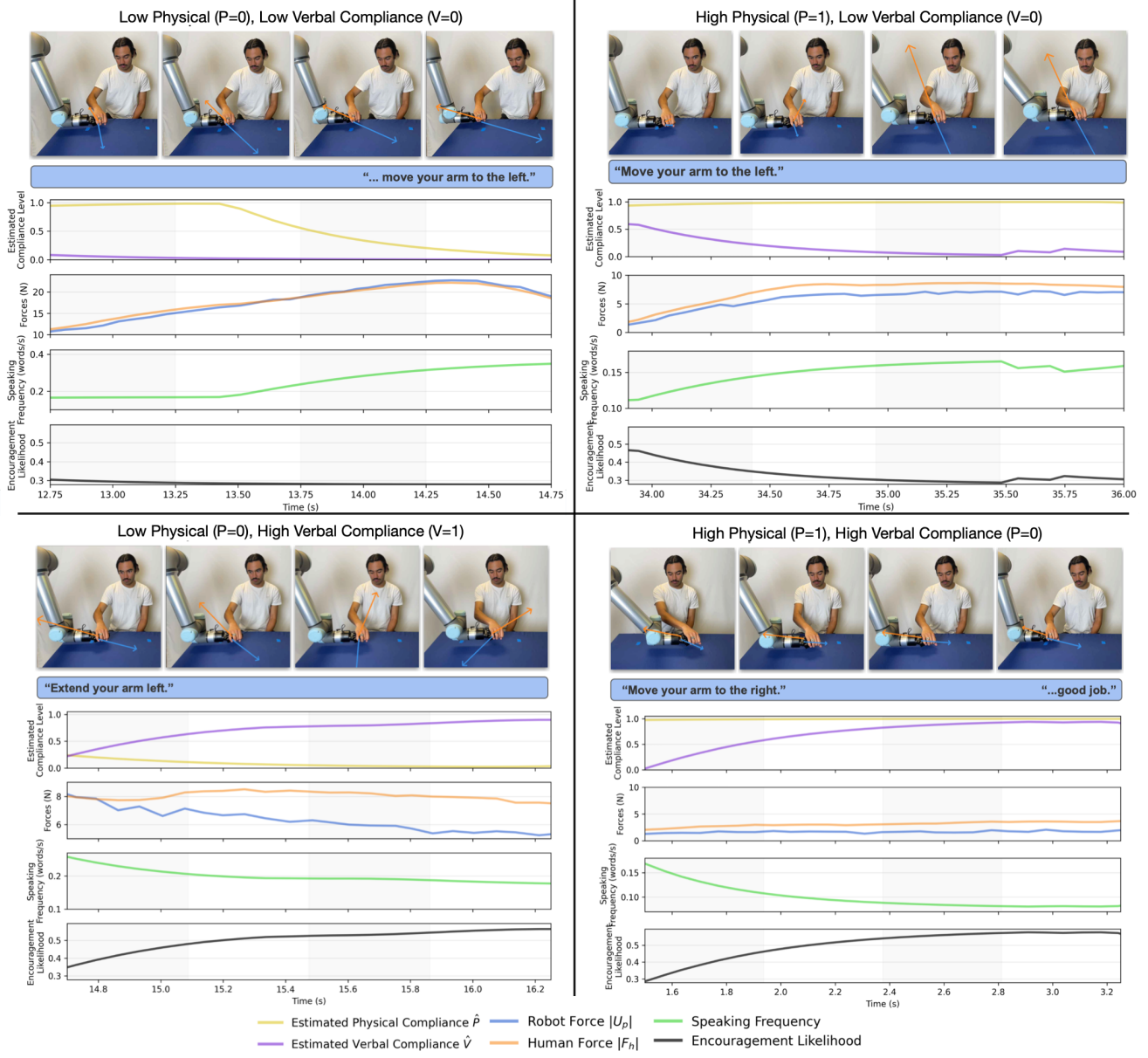


Figure 8: Examples of our Robot Guidance Controller adapting physical and verbal guidance across four compliance regimes. Each quadrant shows a time snippet of a single user trial under different combinations of physical (P) and verbal (V) compliance states. In the low compliance regime (0, 0), the controller increases speaking frequency and delivers strongly directive utterances while maintaining high corrective force. As verbal compliance increases (0, 1), speech becomes less frequent and language remains instructive, while force is moderated. In the reverse case (1, 0), physical guidance dominates, and verbal cues remain frequent but more redundant. Under full compliance (1, 1), the controller decreases both force and speaking frequency, and transitions toward encouraging feedback, matching expert therapist behavior observed (Figure 17). These examples highlight the system’s real-time adaptation in both intensity and content of guidance, driven by compliance estimation and optimization. For full video demonstration and results, see our online appendix.¹

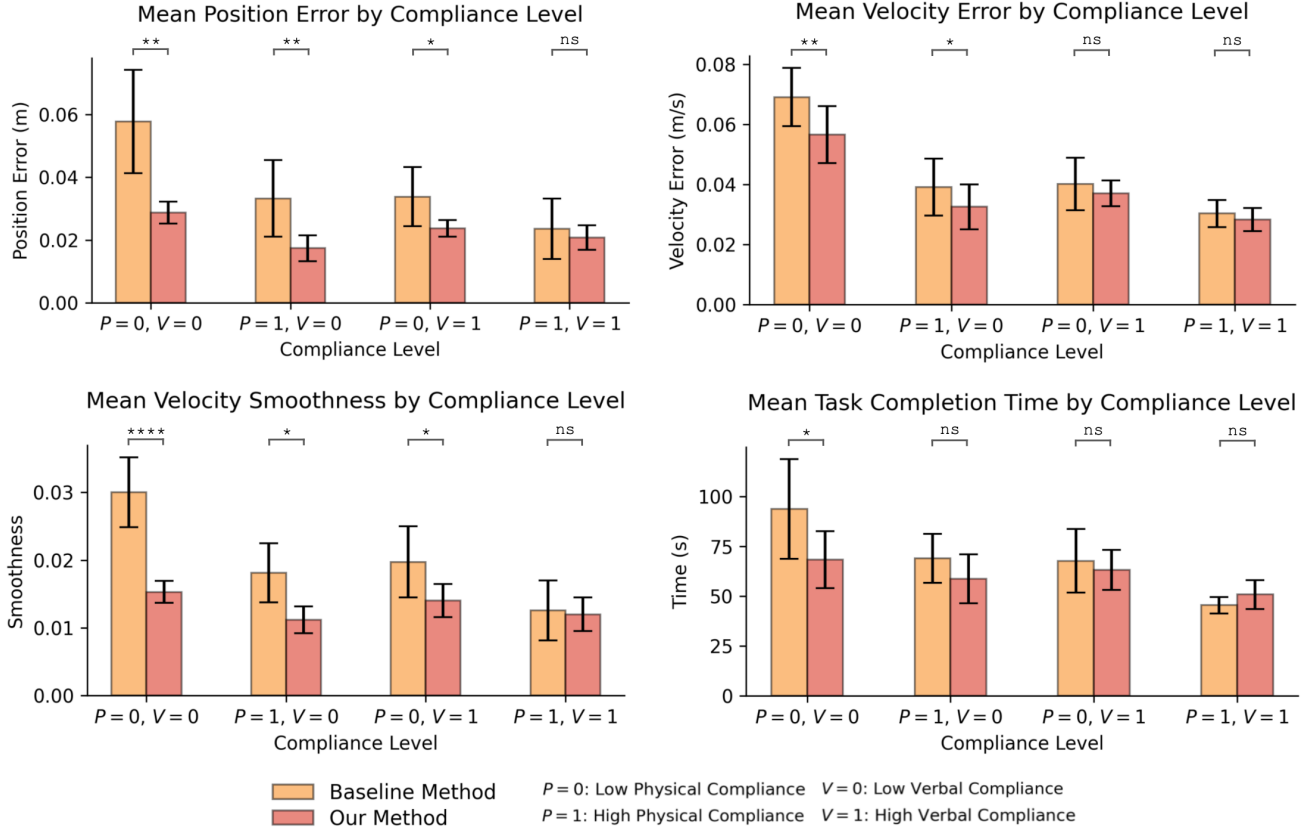


Figure 9: Comparison between our adaptive Robot Guidance Controller (red) and the fixed-weight baseline controller (orange) across all four compliance regimes. Each subplot presents a separate evaluation metric: position error (top left), velocity error (top right), velocity smoothness (bottom left), and task completion time (bottom right). Bars are grouped by compliance level: combinations of physical (P) and verbal (V) compliance ranging from full noncompliance ($P=0, V=0$) to full compliance ($P=1, V=1$). Error bars indicate 95% confidence intervals. Statistical significance is marked above each pairwise comparison (* $p < 0.05$, ** $p < 0.01$, **** $p < 0.0001$, ns = not significant). Our method outperforms the baseline in low-compliance regimes, where adaptive reallocation of guidance helps compensate for unattended modalities; differences taper under full compliance as both methods converge near ceiling performance.

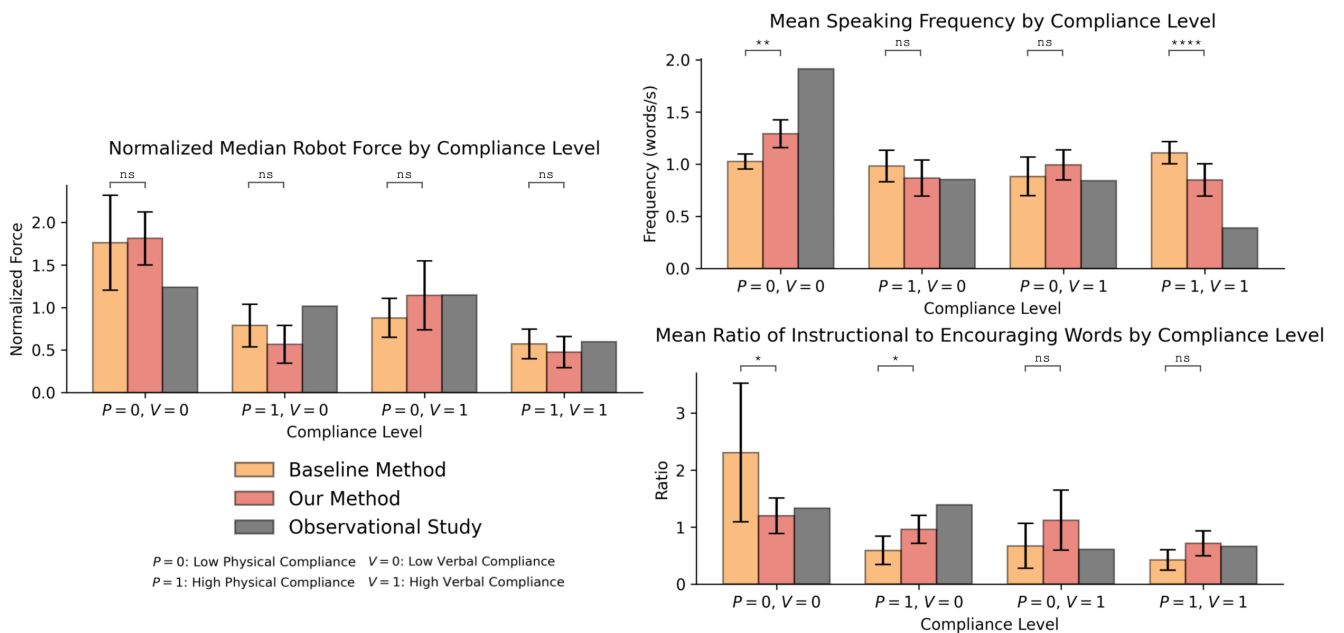


Figure 10: Comparison of robot behavior under the baseline method (orange), our method (red), and the expert therapist from the observational study (gray) across all compliance regimes. Subplots report: normalized median robot force (left), mean speaking frequency (top right), and the mean ratio of instructional to encouraging words (bottom). Bars are grouped by compliance level, with physical (P) and verbal (V) compliance levels annotated below each cluster. Error bars indicate 95% confidence intervals. Statistical significance is marked above each pairwise comparison (* $p < 0.05$, ** $p < 0.01$, **** $p < 0.0001$, ns = not significant). Our method reproduces therapist-like speech behavior more consistently than the baseline, particularly in both speaking frequency and directive balance, while force levels remain comparable across methods.

4 Method

4.1 Notation

$x, \dot{x}, \ddot{x} \in \mathbb{R}^m$: End-effector pose, velocity, and acceleration in the m -dimensional operational space (Sec. 4.3).

$M \in \mathbb{R}^{m \times m}$: Positive-definite virtual inertia matrix in admittance model (Sec. 4.3).

$B \in \mathbb{R}^{m \times m}$: Positive-definite virtual damping matrix in admittance model (Sec. 4.3).

$U_p, U_v \in \mathbb{R}^m$: Physical and verbal guidance wrenches generated by the controller (Sec. 4.4).

$F_h \in \mathbb{R}^m$: Wrench applied by the human, measured at the robot end-effector (Sec. 4.4).

$\delta \in \mathbb{R}^m$: Disturbance $\delta = F_h - U_v$ between the human's realized wrench and the virtual wrench requested through language (Sec. 4.4).

$x_{\text{ref}}, \dot{x}_{\text{ref}} \in \mathbb{R}^m$: Reference pose and tangential velocity (Sec. 4.5).

$e, \dot{e} \in \mathbb{R}^m$: Position and velocity tracking errors: $e = x_{\text{ref}} - x$, $\dot{e} = \dot{x}_{\text{ref}} - \dot{x}$ (Sec. 4.6).

$K_p, K_v \in \mathbb{R}^{m \times m}$: Proportional gain matrices for the physical and verbal PD blocks (Sec. 4.6).

$B_p, B_v \in \mathbb{R}^{m \times m}$: Derivative (damping) gain matrices in the corresponding PD blocks (Sec. 4.6).

$A_p, A_v \in [0, 1]$: Time-varying physical and verbal admittance weights; satisfies $A_p + A_v = 1$ (Sec. 4.6).

$\hat{P}, \hat{V} \in [0, 1]$: Estimates of physical and verbal compliance (Sec. 4.7).

$c_p, c_v \in \mathbb{R}$: Instantaneous costs of physical and verbal guidance (Sec. 4.8).

$\sigma \in \mathcal{L}$: Utterance, chosen from a finite set of phrases \mathcal{L} (Sec. 4.9).

4.2 Overview: Robot Guidance Controller

The Robot Guidance Controller operates in two nested loops. The inner loop is the fixed-rate admittance controller of Sec. 4.3, which converts a commanded wrench U into task-space motion. The outer loop, executed once per cycle, is as follows:

First, the current end-effector pose x is projected onto the reference trajectory, yielding the target state $(x_{\text{ref}}, \dot{x}_{\text{ref}})$ described in Sec. 4.5. The tracking errors e and \dot{e} that result feed two proportional-derivative blocks, producing nominal corrective wrenches for the physical and verbal channels as defined in Sec. 4.6. Force

and kinematic observations update the Bayesian compliance filter, providing the physical and verbal compliance estimates (\hat{P}, \hat{V}) in Sec. 4.7. These probabilities parameterize the quadratic program of Sec. 4.8, which returns adaptive weights (A_p, A_v) and thus the dual-channel wrenches U_p and U_v . Finally, the verbal wrench is rolled forward over a short horizon and converted into an utterance σ via the cross-modal force-language model of Sec. 4.9. The pair (U_p, σ) constitutes the actionable command issued to the human-robot interface, while the passivity result of Sec. 4.10 guarantees that this loop remains energetically safe for any admissible human response.

Algorithm 1 presents the complete control flow, detailing how these components integrate to provide adaptive physical and verbal guidance. The subsequent sections detail each component of this algorithm.

4.3 Task-Space Dynamics Model

We model the coupled robot–human system in task space by imposing a virtual admittance on the robot end-effector. Let

$$x \in \mathbb{R}^m, \quad \dot{x} = \frac{dx}{dt}, \quad \ddot{x} = \frac{d^2x}{dt^2} \quad (1)$$

denote the end-effector pose, velocity, and acceleration in an m -dimensional operational space ($m = 6$ for a full Cartesian wrench). The equation of motion governing the end-effector dynamics follows the general form $M\ddot{x} + B\dot{x} = Q$, where $Q \in \mathbb{R}^m$ represents the total generalized forces acting on the system. In our human-robot interaction context, these generalized forces comprise both the robot's commanded wrench and the human's applied force, yielding the linear admittance model:

$$\underbrace{M\ddot{x} + B\dot{x}}_{\substack{\text{Physical} \\ \text{System}}} = \underbrace{U_p + F_h}_{\substack{\text{Desired} \\ \text{Behavior}}} \quad (2)$$

where $M \in \mathbb{R}^{m \times m}$ and $B \in \mathbb{R}^{m \times m}$ are robot parameters that are positive-definite inertia and damping matrices (Appendix A.2), $U_p \in \mathbb{R}^m$ is the commanded wrench given to the robot to provide physical guidance, and $F_h \in \mathbb{R}^m$ is the wrench applied by the patient. Equation (2) is integrated in real time by the low-level velocity controller [6, 11].

4.4 Dual-Channel Decomposition

We extend (2) to include verbal guidance. Because verbal guidance is delivered as verbal utterances, we leverage the bi-directional force-to-language mapping [23]. We introduce *virtual* wrench $U_v \in \mathbb{R}^m$ generated by the controller. U_v represents a virtual force given to the patient in the form of utterances, which is described in Section 4.9.

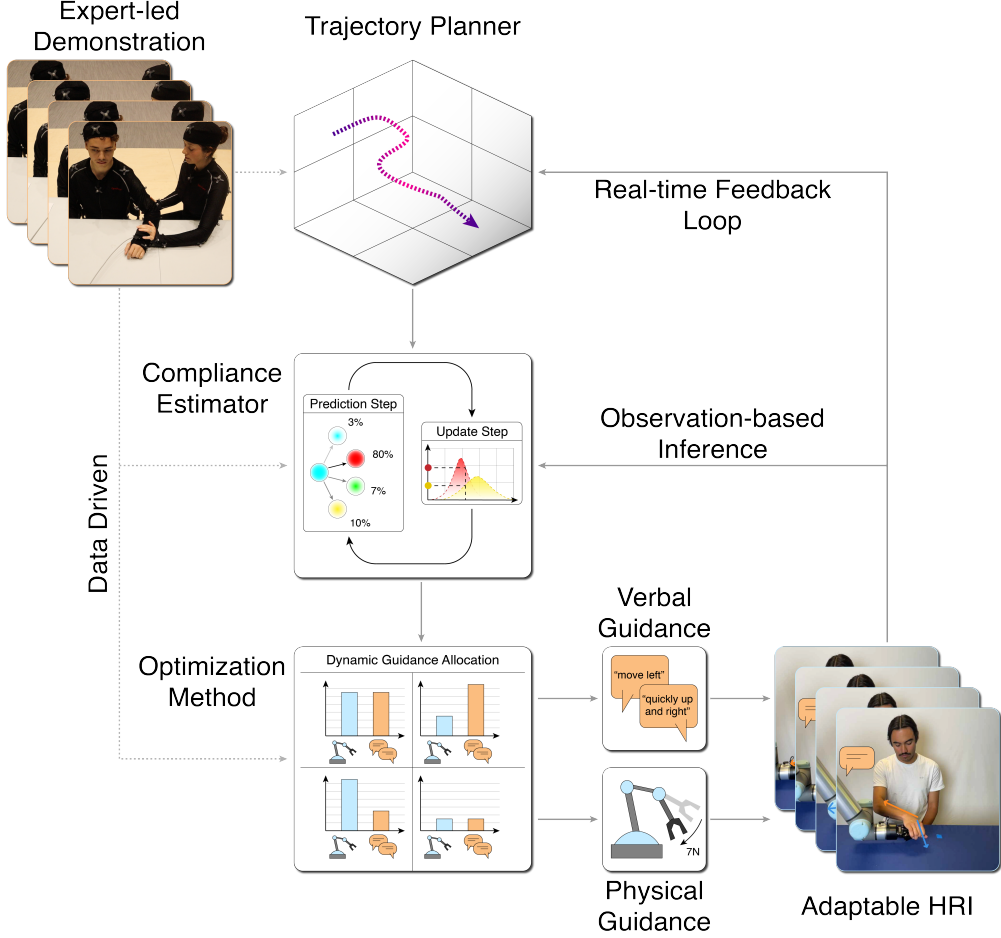


Figure 11: Visual summary of the Robot Guidance Controller for optimal physical and verbal guidance. Expert-led demonstrations generate reference trajectories, and inform module design and parameters. The Trajectory Planner outputs desired motion, while a Bayesian Compliance Estimator infers human receptiveness to different guidance modalities in real time. Based on these estimates, the Optimization Method dynamically allocates guidance effort between physical forces and verbal instructions. The Robot Guidance Controller enables a closed-loop feedback system that provides contextually appropriate, multimodal guidance, enabling real-time adaptive human-robot interaction.

As illustrated in Figure 13, the human’s reaction F_h to a verbal instruction U_v results in a cognitive interpretation and delay (referred to as residual δ), defined as

$$\delta := F_h - U_v. \quad (3)$$

Substituting $F_h = U_v + \delta$ into (2) yields

$$M\ddot{x} + B\dot{x} = U_p + U_v + \delta. \quad (4)$$

We define

$$U := U_p + U_v, \quad (5)$$

so that the overall task-space behavior is described by

$$M\ddot{x} + B\dot{x} = U + \delta, \quad (6)$$

With this formulation, the U_v terms cancel exactly, leaving the physical dynamics unchanged.

The controller’s role is therefore to allocate, at every cycle, the corrective effort between the physical channel (U_p) and the verbal channel (U_v). The optimization governing this allocation is detailed in Section 4.8, and Section 4.10 proves that closed-loop passivity is preserved for all admissible δ .

4.5 Reference Trajectory Generation

To supply the feedback laws with a task-level target we extract a reference curve γ from the therapist-only trial recorded during observational data collection. At every control step the current end-effector pose $x(t)$ is projected to the nearest point on γ ; the resulting position and its tangential velocity constitute $(x_{\text{ref}}(t), \dot{x}_{\text{ref}}(t))$. All preprocessing and projection details are described in Appendix A.1.

Algorithm 1 Robot Guidance Controller

Require: Reference trajectory γ , control gains (K_p, B_p, K_v, B_v) , robot dynamics (M, B)

Ensure: Physical guidance U_p and verbal utterance σ

- 1:
- 2: **while** task not complete **do**
- 3: Measure end-effector pose $x(t)$ and velocity $\dot{x}(t)$ ▷ Measurement Phase
- 4: Measure human interaction force $F_h(t)$
- 5: ▷ Reference Projection
- 6: $s^*(t) \leftarrow \arg \min_s \|x(t) - \gamma(s)\|$
- 7: $x_{\text{ref}}(t) \leftarrow \gamma(s^*(t))$
- 8: $\dot{x}_{\text{ref}}(t) \leftarrow \gamma'(s^*(t))$
- 9: ▷ Tracking Error
- 10: $e(t) \leftarrow x_{\text{ref}}(t) - x(t)$
- 11: $\dot{e}(t) \leftarrow \dot{x}_{\text{ref}}(t) - \dot{x}(t)$
- 12: ▷ Compliance Estimation
- 13: $z_t \leftarrow \begin{bmatrix} e(t) \\ \dot{e}(t) \end{bmatrix}$
- 14: Update belief π_t via Bayesian filter
- 15: $\hat{P}_t \leftarrow \pi_{10,t} + \pi_{11,t}$
- 16: $\hat{V}_t \leftarrow \pi_{01,t} + \pi_{11,t}$
- 17: ▷ Cost Computation
- 18: $c_p(t) \leftarrow \frac{1}{2}(\hat{P}_t + \hat{V}_t)$
- 19: $c_v(t) \leftarrow 1 - \hat{V}_t$
- 20: ▷ Weight Allocation
- 21: $A_p^*(t) \leftarrow c_v(t)/(c_p(t) + c_v(t))$
- 22: $A_v^*(t) \leftarrow c_p(t)/(c_p(t) + c_v(t))$
- 23: ▷ Control Laws
- 24: $U_p(t) \leftarrow K_p e + B_p \dot{e} - A_p^* F_h$
- 25: $U_v(t) \leftarrow K_v e + B_v \dot{e} - A_v^* F_h$
- 26: ▷ Force-to-Language
- 27: Compute profile \mathbf{u}_v over horizon T
- 28: $\sigma \leftarrow \Psi(\mathbf{u}_v)$
- 29: ▷ Actuation
- 30: Apply U_p to robot
- 31: Speak utterance σ
- 32: Update dynamics: $M\ddot{x} + B\dot{x} = U_p + F_h$
- 33: **end while**

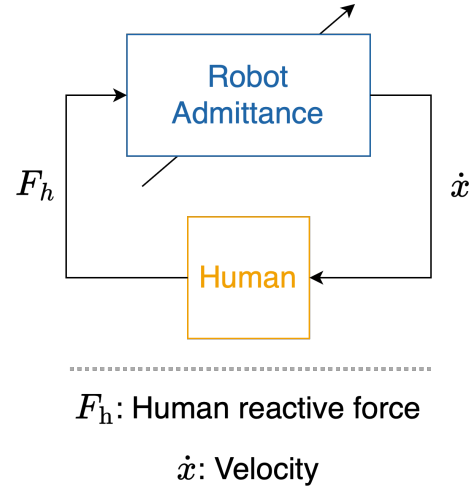


Figure 12: Conventional Variable Admittance human-robot Interaction control loop depicting the high-level relationship between the robot admittance controller and human input. The diagram illustrates how human reactive force (F_h), resulting from variable human impedance characteristics, influences the system dynamics, while the controller regulates end-effector velocity (\dot{x}) through admittance parameters that must adapt to changing human biomechanical properties.

4.6 Control Laws

At every control cycle the controller (i) computes nominal corrective wrenches from the tracking error and (ii) modulates those wrenches with adaptive weights to apportion guidance between the robot and the human.

Let

$$e(t) = x_{\text{ref}}(t) - x(t), \quad (7)$$

$$\dot{e}(t) = \dot{x}_{\text{ref}}(t) - \dot{x}(t) \quad (8)$$

denote the instantaneous tracking error, where $x_{\text{ref}}(t)$ is the task-level reference pose supplied by the trajectory generator. We employ independent proportional-derivative blocks to convert this error into nominal corrective wrenches for the two actuators:

$$\text{PD}_p(e) = K_p e + B_p \dot{e}, \quad (9)$$

$$\text{PD}_v(e) = K_v e + B_v \dot{e}, \quad (10)$$

where $K_p, B_p, K_v, B_v \in \mathbb{R}^{m \times m}$ are constant, positive-definite gains identified offline from expert demonstrations in Observational Study (Appendix A.3).

The human's measured interaction wrench $F_h \in \mathbb{R}^m$ is filtered through scalar, time-varying adaptive weights $A_p(t), A_v(t) \in [0, 1]$ with the convex-combination constraint:

$$A_p(t) + A_v(t) = 1. \quad (11)$$

A smaller value denotes greater admittance (the actuator yields to the human), while a larger value denotes

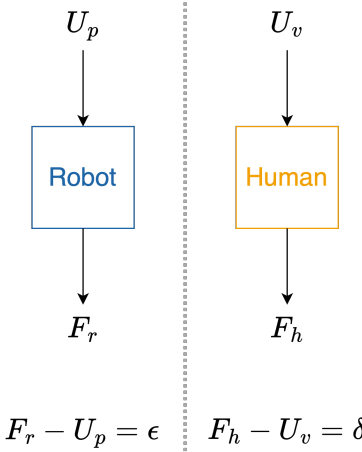


Figure 13: Manifestation of physical and verbal control inputs in human-robot interaction. In a typical robot controller, a robot receives a commanded wrench U_p , which manifests as an actuator force F_r . In a human setting, when a human receives a verbal instructions U_v (converted to spoken utterances via force-to-language mapping [23]), it manifests as a human wrench F_h . In practice, the $\epsilon = F_r - U_p$ is close to 0. In contrast, the human exhibits a residual disturbance $\delta = F_h - U_v$, reflecting cognitive interpretation and delay (referred as residual).

greater guidance authority. Incorporating these weights yields the channel control laws

$$U_p(t) = \text{PD}_p(e(t)) - A_p(t)F_h(t), \quad (12)$$

$$U_v(t) = \text{PD}_v(e(t)) - A_v(t)F_h(t). \quad (13)$$

Because the weights satisfy (11), their superposition $U_p(t) + U_v(t)$ equals the single-actuator wrench that would result from combining the two PD terms and admitting F_h with unit-gain. Hence the dual-actuator decomposition reallocates, but does not alter, the total wrench driving the admittance dynamics (2).

4.7 Compliance Estimation

As direct measurement of human compliance is infeasible, we utilize a recursive Bayesian estimation framework [26, 12] to infer compliance states from observable task performance.

Let

$$X_t = (P_t, V_t) \in \{0, 1\}^2 \quad (14)$$

denote the joint compliance state at time t , where P_t and V_t represent individual physical and verbal compliance levels. As per our observational study, we confine the compliance levels to a binary state where 0 represents low compliance and 1 represents high compliance (Section A). The system assumes X_t evolves as a first-order Markov process conditioned on the previous state X_{t-1} and control inputs U_p, U_v .

We define our observation vector $z_t \in \mathbb{R}^n$ as

$$z_t = \begin{bmatrix} e(t) \\ \dot{e}(t) \end{bmatrix} = \begin{bmatrix} x_{\text{ref}}(t) - x(t) \\ \dot{x}_{\text{ref}}(t) - \dot{x}(t) \end{bmatrix}, \quad (15)$$

where $e(t)$ and $\dot{e}(t)$ quantify positional and velocity deviations from the reference trajectory. Larger tracking errors correlate with lower compliance, while smaller errors suggest higher adherence to guidance.

We represent the belief over the four possible joint states of X_t by the probability vector

$$\pi_t = [\pi_{00,t}, \pi_{01,t}, \pi_{10,t}, \pi_{11,t}], \quad (16)$$

where $\pi_{ij,t} = \mathbb{P}(X_t = (i,j)|z_t)$ is the probability of the compliance levels given the observations. The estimator then operates in two stages:

Prediction Step. First, the prior $\tilde{\pi}_{ij,t}$ is computed by propagating the previous belief $\pi_{ij,t}$ into the future using the Chapman–Kolmogorov equation:

$$\tilde{\pi}_{ij,t} = \mathbb{P}(X_t = (i,j)|z_{t-1}, U_{t-1}) \quad (17)$$

$$= \sum_{X_{t-1}} \mathbb{P}(X_t = (i,j)|X_{t-1}, U_{t-1}) \pi_{ij,t-1}. \quad (18)$$

We parameterize the 4×4 transition probabilities as a softmax over linear functions of the control input, and the corresponding weights are fit from the annotated data (See Appendix A.4 for more details).

Update Step. Next, we incorporate the new observations z_t to obtain the posterior $\pi_{ij,t}$ via Bayes' rule:

$$\pi_{ij,t} = \frac{\mathbb{P}(z_t|X_t = (i,j))\tilde{\pi}_{ij,t}}{\sum_{X_t} \mathbb{P}(z_t|X_t)\mathbb{P}(X_t|z_{t-1}, U_{t-1})}. \quad (19)$$

Here, we model each likelihood $\mathbb{P}(z_t|X_t = (i,j))$ as a multivariate Gaussian $\mathcal{N}(z_t; \mu_{ij}, \Sigma_{ij})$ with mean μ_{ij} and covariance Σ_{ij} estimated from the collected data (Appendix A.5).

Finally, we define the inferred compliance levels \hat{P}_t, \hat{V}_t as the marginal probabilities of full compliance:

$$\hat{P}_t = \mathbb{P}(P_t = 1|z_t) = \pi_{10,t} + \pi_{11,t}, \quad (20)$$

$$\hat{V}_t = \mathbb{P}(V_t = 1|z_t) = \pi_{01,t} + \pi_{11,t}. \quad (21)$$

These estimates provide real-time measures of the human's physical and verbal responsiveness that are used to inform the controller's adaptive allocation between physical and verbal guidance.

4.8 Adaptive Weight Allocation

To adaptively adjust the relative amounts of physical and verbal guidance, the weights $A_p(t)$ and $A_v(t)$ introduced in (12) are updated online by solving a point-wise quadratic optimization expressed in terms of *costs* of providing physical and verbal guidance.

Let $\hat{P}(t), \hat{V}(t) \in [0, 1]$ denote, respectively, the physical and verbal compliance estimates produced by the

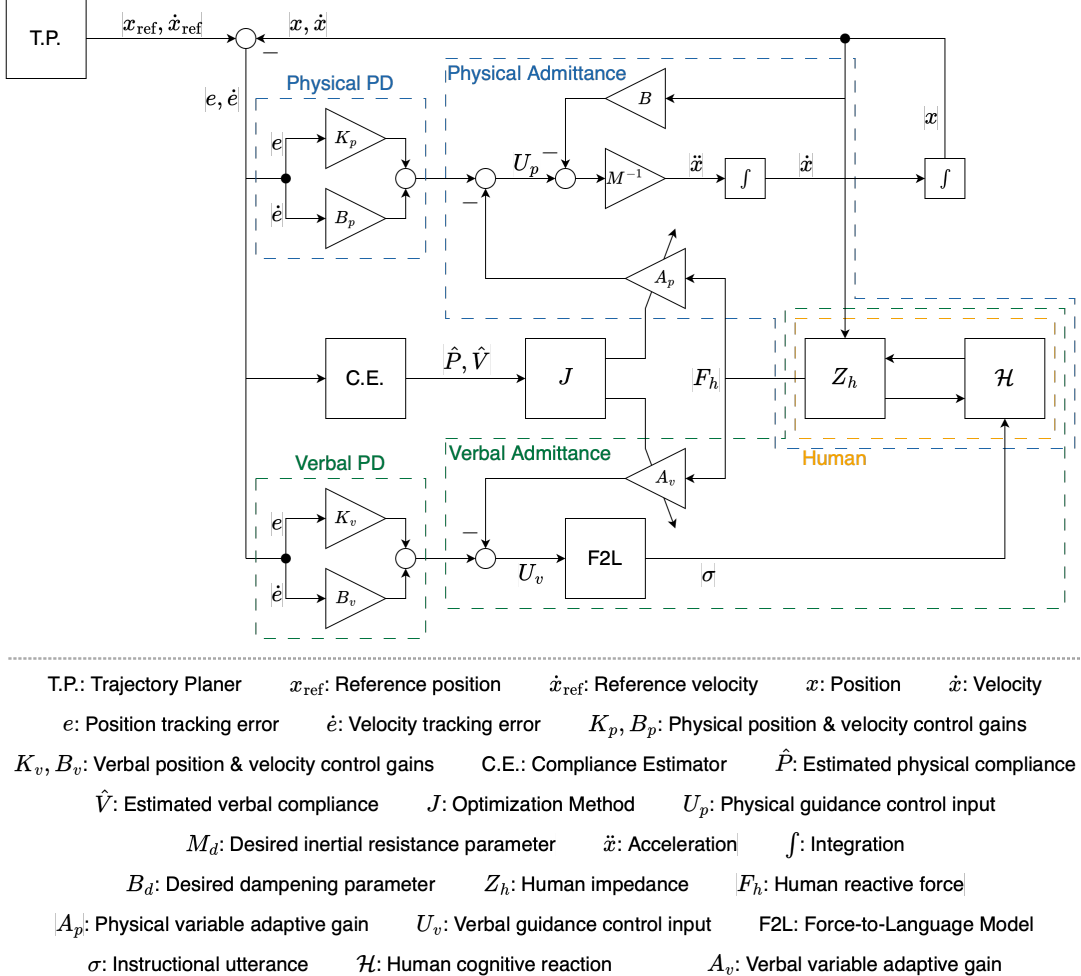


Figure 14: Control loop of our Robot Guidance Controller. The diagram illustrates how position and velocity tracking errors (e, \dot{e}) are processed through parallel physical and verbal PD controllers with dedicated gain parameters (K_p, B_p, K_v, B_v). The optimization method (J) uses compliance estimates to determine appropriate variable admittance gains (A_p, A_v) that modulate the physical guidance control input (U_p) and verbal guidance control input (U_v). These gains continuously adapt to the variable human impedance (Z_h) and human cognitive reaction (H), with verbal inputs converted to instructional utterances (σ) through a Force-to-Language (F2L) model that accounts for varying levels of human receptiveness.

Bayesian filter described in Section 4.7. We assign instantaneous, positive costs

$$c_p(t) = \phi_p(\hat{P}(t), \hat{V}(t)), \quad (22)$$

$$c_v(t) = \phi_v(\hat{P}(t), \hat{V}(t)) \quad (23)$$

with the following monotonicity properties:

- The cost of physical guidance c_p increases as the human’s physical or verbal compliance increases (the robot should push harder only when effective).
- The cost of verbal guidance c_v increases as verbal compliance decreases (talking more is wasteful if instructions are consistently ignored).

These properties are derived from our observations described in Appendix A. The specific functional choice for ϕ_* is left to experimental tuning, in our case we use

$$\phi_p(\hat{P}, \hat{V}) = \frac{1}{2}(\hat{P} + \hat{V}), \quad (24)$$

$$\phi_v(\hat{P}, \hat{V}) = 1 - \hat{V}, \quad (25)$$

which satisfy the monotonicity properties outlined above.

At each control step we formulate an objective

$$J = c_p A_p^2 + c_v A_v^2, \quad (26)$$

representing the total cost of applying physical and verbal guidance. Intuitively, when the cost of one particular guidance is higher, we’d like that control input to admit *more* to the human’s wrench, as we cannot afford to correct for the human’s actions. Alternatively, if the cost of a particular guidance is lower, then we can afford to admit *less* to the human’s wrench and provide more corrective control.

Recall the constraint given by (11), at each step we solve:

$$\min_{A_p, A_v} J = \min_{A_p, A_v} (c_p A_p^2 + c_v A_v^2) \quad (27)$$

$$\text{s.t. } A_p + A_v = 1, \quad A_p \geq 0, A_v \geq 0. \quad (28)$$

To solve this optimization, we first substitute the constraint $A_v = 1 - A_p$ into the objective:

$$J(A_p) = c_p A_p^2 + c_v (1 - A_p)^2. \quad (29)$$

Then minimizing $J(A_p)$ directly is sufficient. Taking the derivative of $J(A_p)$ with respect to A_p and setting it to zero yields

$$\frac{dJ}{dA_p} = c_p A_p - c_v (1 - A_v) = 0. \quad (30)$$

Solving for A_p , we have

$$c_p A_p = c_v (1 - A_p), \quad (31)$$

$$A_p(c_p + c_v) = c_v, \quad (32)$$

$$A_p = \frac{c_v}{c_p + c_v}. \quad (33)$$

Consequently, the optimal adaptive weights A_p^*, A_v^* are given by

$$A_p^*(t) = \frac{c_v(t)}{c_p(t) + c_v(t)}, \quad (34)$$

$$A_v^*(t) = \frac{c_p(t)}{c_p(t) + c_v(t)}, \quad (35)$$

which can be substituted directly into the control laws given by (12):

$$U_p(t) = \text{PD}_p(e(t)) - \frac{c_v(t)}{c_p(t) + c_v(t)} F_h(t), \quad (36)$$

$$U_v(t) = \text{PD}_v(e(t)) - \frac{c_p(t)}{c_p(t) + c_v(t)} F_h(t), \quad (37)$$

yielding our final adaptive formulas for the physical and verbal control inputs.

4.9 Force to Language

To translate the virtual wrench U_v into a verbal cue, we employ the cross-modal force-to-language model introduced by [23], which embeds force profiles and natural-language phrases into a shared latent space.

Following [23], an utterance must encode three attributes of the intended human action: magnitude, direction, and duration. We therefore project the controller forward over a fixed horizon T while holding the current compliance estimates \hat{P}, \hat{V} constant. Assuming the human tracks the verbal request, we substitute $F_h = U_v$ into the control law given by (13):

$$U_v(\tau) = K_v e(\tau) + B_v \dot{e}(\tau) - A_v U_v(\tau), \quad (38)$$

which reduces to:

$$U_v(\tau) = \frac{K_v e(\tau) + B_v \dot{e}(\tau)}{1 + A_v}, \quad \tau \in [t, t + T]. \quad (39)$$

Equation (39) is evaluated at $N = T/\Delta t$ uniform samples to yield the profile

$$\mathbf{u}_v = [U_v(t), \dots, U_v(t + T)], \quad (40)$$

which is fed into the model provided by [23]. The model embeds the profile into a joint force-language latent space and outputs the closest utterance

$$\sigma = \Psi(\mathbf{u}_v) \in \mathcal{L}, \quad (41)$$

where \mathcal{L} is a finite library of therapist-style phrases (e.g. “*push gently to the right*”). The resulting utterance is then delivered through a speech synthesizer to provide verbal guidance to the patient.

4.10 Passivity

Passivity guarantees that the closed-loop robot cannot generate net mechanical energy and therefore remains Lyapunov stable when coupled to a passive environment such as a human arm [16, 27]. We prove that our proposed controller is *output-strictly passive* with respect to the port variables (F_h, \dot{x}).

Throughout, we recall the error definition

$$e(t) = x_{\text{ref}}(t) - x(t), \quad \dot{e}(t) = \dot{x}_{\text{ref}}(t) - \dot{x}(t), \quad (42)$$

where the reference state $(x_{\text{ref}}, \dot{x}_{\text{ref}})$ is obtained at each control cycle by projecting the current end-effector pose onto the therapist-demonstrated curve γ (Sec. 4.5). By construction of this nearest-point projection we have, for all t ,

$$e(t)^{\top} \dot{x}_{\text{ref}}(t) = 0. \quad (43)$$

Define the candidate storage function

$$S(t) = \frac{1}{2} \dot{x}^{\top} M \dot{x}(t) + \frac{1}{2} e(t)^{\top} K_p e(t), \quad (44)$$

which combines the kinetic energy [7, 19] of the effective inertia $M \succ 0$ with the potential energy stored in the proportional term $K_p \succ 0$.

Theorem 1. *Let $M \succ 0$, $B \succ 0$, $K_p \succ 0$ and $B_p \succ 0$, and assume the admittance dynamics (2) together with the physical control law*

$$U_p = K_p e + B_p \dot{e} - A_p F_h, \quad 0 \leq A_p(t) \leq 1, \quad \forall t, \quad (45)$$

where $A_p + A_v = 1$ as in (11). Then for every $t \geq 0$

$$S(t) - S(0) \leq \int_0^t F_h(\tau)^{\top} \dot{x}(\tau) d\tau. \quad (46)$$

Hence the closed loop is passive with input F_h and output \dot{x} .

The proof of Theorem 1 is provided in Appendix B.

5 Data and Code Availability

The entire dataset, including observational data and user study results, is publicly available in our online repository at <https://robot-guidance-controller.github.io/>. The code for the Robot Guidance Controller is available at <https://github.com/robot-guidance-controller/robot-guidance-controller/>.

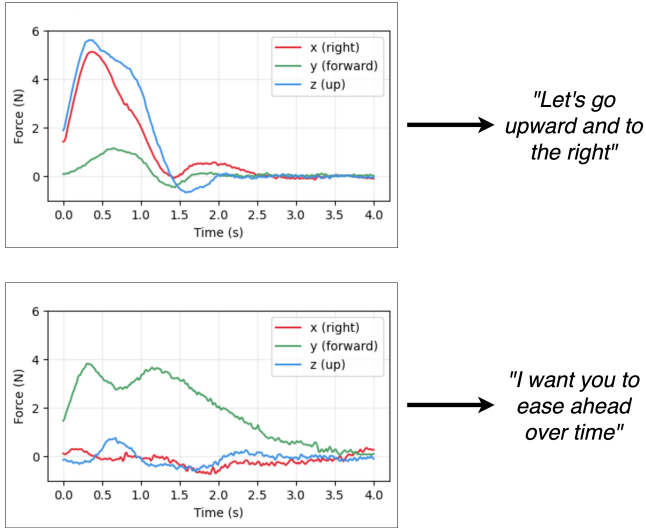


Figure 15: Example translations from force profiles to instructional utterances using the cross-modality force-language model introduced in [23]. Each plot shows a 3D force profile over time, with the x , y , and z components shown in red, green, and blue, respectively. The top example corresponds to the utterance “*You should go ahead softly*” and features low overall force magnitude, peaking at around 8 N, with the y -axis (green) as the only dominant component—consistent with a soft motion forward. In contrast, the bottom example translates to the phrase “*Harshly push to the right and forward*” and exhibits a significantly higher peak force of approximately 17.5 N, with both the x and y components (red and green) being prominent while the z component remains near zero—corresponding to a strong diagonal push in the forward-right direction. These examples demonstrate the model’s ability to map time varying force profiles into semantically grounded natural language directives.

References

- [1] Haruhiko Asada and Yasuo Asari. The direct teaching of tool manipulation skills via the impedance identification of human motion. In *Proceedings of IEEE International Conference on Robotics and Automation*, pages 1269–1274. IEEE, 1988.
- [2] Christopher G Atkeson and Stefan Schaal. Robot learning from demonstration. In *ICML*, volume 97, pages 12–20, 1997.
- [3] Ivan Diaz, Jorge J Gil, and Emilio Sanchez. Rehabilitation robots for the treatment of sensorimotor deficits: A neurophysiological perspective. *Journal of NeuroEngineering and Rehabilitation*, 15(1):1–15, 2018.
- [4] Brian R Duffy and Gina Joue. The paradox of social robotics: A discussion. In *AAAI Fall Symposium on Machine Ethics*, pages 22–24, 2005.
- [5] Juan Fasola and Maja J Mataric. A socially assistive robot exercise coach for the elderly. *Journal of Human-Robot Interaction*, 2(2):3–32, 2013.
- [6] Federica Ferraguti, Cristian Secchi, and Cesare Fantuzzi. A variable admittance control strategy for stable physical human–robot interaction. *The International Journal of Robotics Research*, 32(8):949–968, 2013.
- [7] Sami Haddadin, Alin Albu-Schaffer, and Gerd Hirzinger. Safe, stable and intuitive control for physical human-robot interaction. pages 3383–3388, 2009.
- [8] Chien-Ming Huang and Bilge Mutlu. Multivariate evaluation of interactive robot systems. *Autonomous Robots*, 37(4):335–349, 2014.
- [9] Nam Kim, Hyomin Shin, Hyunjun Sim, and Gyeore Park. Variable admittance control based on human–robot collaboration observer using frequency analysis for sensitive and safe interaction. *Sensors*, 21(5):1899, 2021.
- [10] Hermano Igo Krebs, Neville Hogan, Mindy L Aisen, and Bruce T Volpe. Rehabilitation robotics: Performance-based progressive robot-assisted therapy. *Autonomous robots*, 15(1):7–20, 2003.
- [11] Chiara Talignani Landi, Federica Ferraguti, Lorenzo Sabattini, Cristian Secchi, Marcello Bonfè, and Cesare Fantuzzi. Variable admittance control preventing undesired oscillating behaviors in physical human-robot interaction. pages 3611–3616, 2017.
- [12] Yongfeng Li, Giacomo Carboni, Fernando Gonzalez, Domenico Campolo, and Etienne Burdet. Trust-based variable impedance control of human–robot cooperative manipulation. *Robotics and Computer-Integrated Manufacturing*, 86:102667, 2024.
- [13] Sheng Liu and Haruhiko Asada. Transferring manipulative skills to robots: Representation and acquisition of tool manipulative skills using a process dynamics model. 1992.
- [14] Tomás Lozano-Pérez. Robot programming. *Proceedings of the IEEE*, 71(7):821–841, 1983.
- [15] Tomás Lozano-Pérez. Teaching robots by task demonstration. In *Proceedings of the IEEE International Conference on Robotics and Automation*, 1987.
- [16] Shakhzod Mamedov, Stanislav Mikhel, Deepan Muthirayan, Asatur Khurshudyan, Mohamad Kounou, and Dzmitry Tsetserukou. A passivity-based framework for safe physical human–robot interaction. *Robotics*, 12(4):116, 2023.
- [17] Elaine L Miller, Linda Murray, Lorie Richards, Richard D Zorowitz, Tamlyn Bakas, Patricia Clark, and Sandra A Billinger. Comprehensive overview of nursing and interdisciplinary rehabilitation care of the stroke patient: A scientific statement from the american heart association. *Stroke*, 41(10):2402–2448, 2010.
- [18] Bogdan Mocan, Mircea Mocan, Mihaela Fulea, Mihaela Murar, and Horea Feier. Robotics in physical rehabilitation: Systematic review. *Healthcare*, 12(17):1720, 2024.
- [19] Luka Petrovic, Loredana Zollo, and Oussama Khatib. Energy based control for safe human-robot physical interaction. In *2016 International Symposium on Experimental Robotics*, pages 723–733. Springer, 2017.
- [20] David J Reinkensmeyer and James L Patton. Can robots help the learning of skilled actions? *Exercise and Sport Sciences Reviews*, 37(1):43, 2009.
- [21] Stéphane Ross and Drew Bagnell. Efficient reductions for imitation learning. In *Proceedings of the thirteenth international conference on artificial intelligence and statistics*, pages 661–668. JMLR Workshop and Conference Proceedings, 2010.
- [22] Bo Sheng, Yanxin Zhang, Wei Meng, Chao Deng, and Shengquan Xie. The present and future of robotic technology in rehabilitation. *Current Opinion in Neurology*, 29(6):p814–821, 2016.

- [23] Ravi Tejwani, Karl Velazquez, John Payne, Paolo Bonato, and Harry Asada. Cross-modality embedding of force and language for natural human-robot communication. In *Proceedings of Robotics: Science and Systems*, Los Angeles, California, June 2025.
- [24] Yongbiao Wang, Yang Yang, Boyang Zhao, Xinyu Qi, Yuehua Hu, Bing Li, Lining Sun, Long Zhang, and Max Q-H Meng. Variable admittance control based on trajectory prediction of human hand motion for physical human-robot interaction. *Applied Sciences*, 11(12):5651, 2021.
- [25] Qing Wu, Xuejun Zhao, Yan Wang, and Jie Zhang. Variable admittance control for safe physical human–robot interaction considering intuitive human intention. *Mechanism and Machine Theory*, 184:105307, 2023.
- [26] Xinbo Yu, Wei He, Yanan Li, Chengqian Xue, Jianqiang Li, Jianxiao Zou, and Chenguang Yang. Bayesian estimation of human impedance and motion intention for human-robot collaboration. *IEEE Transactions on Cybernetics*, 51(4):1822–1834, 2021.
- [27] Zhiqian Zhang, Marion Leibold, and Martin Buss. Constrained passive interaction control: Leveraging passivity and safety for robot manipulators. *arXiv preprint arXiv:2403.09853*, 2024.

SUPPLEMENTARY MATERIAL

A Observational Study

We conducted an observational study to understand how instructors adapt their guidance to learner behavior. While this approach applies to any instructor-learner interaction, we focused on physical therapy as a representative domain. We collaborated with Spaulding Rehabilitation Hospital and observed the chief therapist providing physical therapy to a patient during shoulder-flexion exercises – a rehabilitation task for improving range of motion. This exercise requires continuous physical contact and verbal communication, making it ideal for studying adaptive guidance. The objective was to observe how a instructor modulates physical and verbal guidance in response to the learner’s compliance levels.

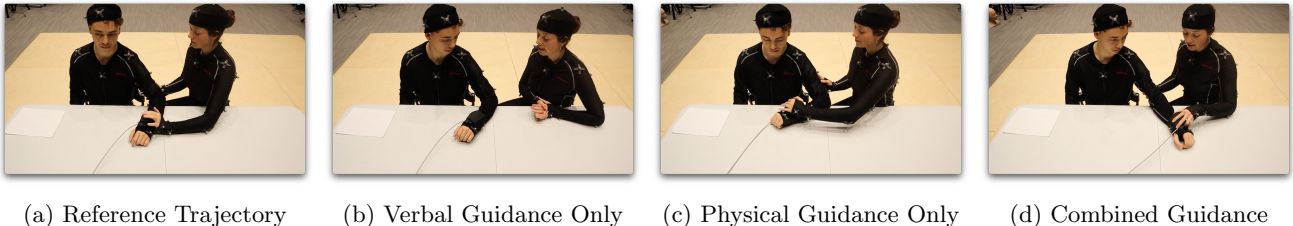


Figure 16: Screenshots of the observational study conducted with Spaulding Rehabilitation Hospital. (a) Therapist executing the shoulder-flexion exercise with the patient remaining passive to record the reference trajectory. (b) Patient performing the exercise with verbal guidance only. (c) Patient performing the exercise with physical guidance only. (d) Patient performing the exercise under combined verbal and physical guidance. Full video demonstration for each of the experimental conditions can be found in our online appendix ¹

For the purposes of our analysis, compliance levels were classified as low or high. The patient was free to vary their compliance at will during each trial. After the session, the patient reviewed the video recording and annotated a timeline indicating, for every instant, their physical and verbal compliance levels.

Conditions Four distinct conditions were established:

1. **Reference Trajectory:** The therapist performed the exercise while the patient remained passive (neither actively complying nor resisting). This provided baseline data for learning reference trajectory ($x_{\text{ref}}, \dot{x}_{\text{ref}}$) and system dynamics parameters (M, B).
2. **Verbal Guidance Only:** The therapist provided only verbal guidance without any physical contact as the patient attempted to follow the trajectory. During these trials, the patient varied their verbal compliance levels. This enabled learning verbal control gains (K_v, B_v).
3. **Physical Guidance Only:** The therapist guided the patient using only physical guidance without verbal cues. During these trials, the patient varied their physical compliance levels. This enabled learning physical control gains (K_p, B_p).
4. **Combined Guidance:** The therapist used both physical and verbal guidance simultaneously. During these trials, the patient varied both physical and verbal compliance levels. This provided data for learning compliance estimation parameters.

We conducted 10 trials for each condition with different compliance level combinations and recorded the therapist’s guidance strategies and patient responses. The systematic variation of compliance levels across conditions allowed us to isolate and identify the key parameters needed for our adaptive controller (detailed derivations in Section 4).

Data Collection We collected multiple data streams during each trial to capture the full interaction between therapist and patient. Motion capture systems tracked 3D positions of the patient’s and therapist’s hands, arms, and torso throughout the exercises. A force sensor attached to the patient’s wrist measured the magnitude and direction

¹Online Appendix showcasing the video demonstration for observational data <https://robot-guidance-controller.github.io/observational-study/>

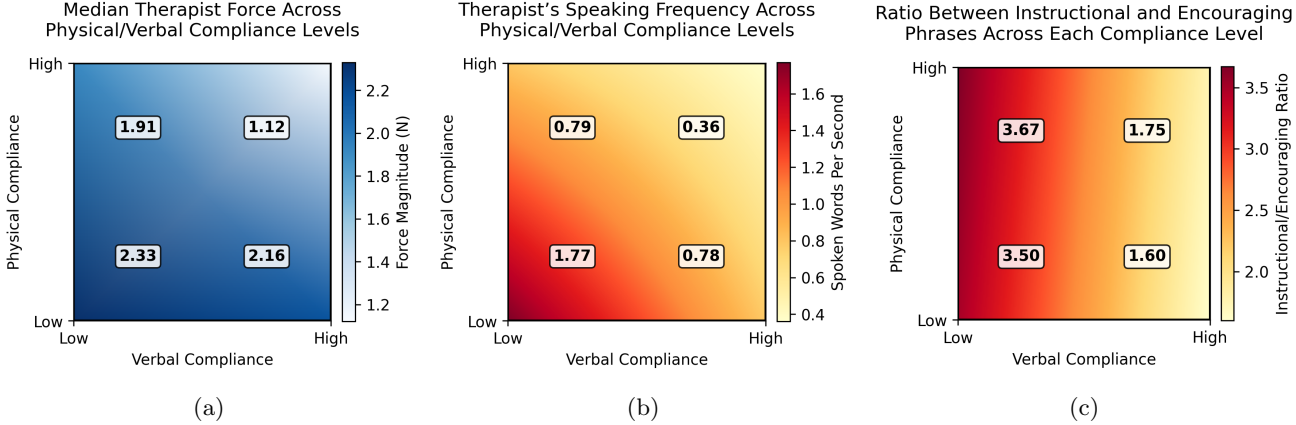


Figure 17: Instructor led guidance patterns observed during therapist-patient interactions. (a) Median force applied decreases from 2.33 N at low compliance ($P=0, V=0$) to 1.12 N at high compliance ($P=1, V=1$). (b) Speaking frequency reduces from 1.77 to 0.36 words/second as compliance improves. (c) Instructional-to-encouraging phrase ratio shifts from 3.67 (predominantly instructional) to 1.60 (more encouraging) with increasing compliance. These patterns demonstrate how expert instructors naturally reduce both physical intervention intensity and instructional explicitness as learner compliance increases - forming the basis for our method.

of interaction forces between therapist and patient. Inertial measurement units (IMUs) recorded acceleration and angular velocity data from the patient’s arm segments.

Additionally, we recorded all therapist speech using a microphone, capturing the content of instructions, speaking frequency, and timing of verbal cues. All data streams were synchronized and annotated with the patient’s self-reported compliance levels at each time instant, enabling us to correlate the therapist’s guidance with the patient’s compliance states.

Observations Analysis of the therapist’s behavior revealed adaptations in physical and verbal guidance based on patient compliance levels, as summarized in Figure 17. The therapist adjusted both physical and verbal guidance in response to the patient’s compliance state. When patient compliance was low (both physical and verbal), the therapist applied higher physical force (2.33 N median) and maintained high speaking frequency (1.77 words per second). As compliance improved, both metrics decreased substantially—force reduced to 1.12 N and speaking frequency to 0.36 words per second when both compliance levels were high.

In particular, the verbal strategy of the therapist evolved beyond frequency modulation. The ratio of instructional to encouraging phrases shifted dramatically with compliance levels: from predominantly instructional language (ratio of 3.67) when physical compliance was low, to encouraging language (ratio of 1.60) when both compliance levels were high. This shift from directive to supportive communication parallels the reduction in physical intervention. These adaptive patterns - where increased compliance triggers reduced physical force, lower speaking frequency, and more encouraging language - directly informed the design of our controller’s optimization strategy to allocate physical and verbal guidance based on real-time compliance estimates (Section 4).

A.1 Reference Trajectory

The reference trajectory was derived from therapist demonstrations during the reference trajectory condition. To capture the ideal motion profile, the therapist performed 12 repetitions of the shoulder flexion exercise while the patient remained passive. The patient’s wrist pose x and velocity \dot{x} was recorded at 200 Hz for a total of 26,328 samples.

We applied the following preprocessing: (1) Each repetition was segmented into individual cycles, defined as the motion from the neutral position to full extension and back. (2) Cycles were temporally aligned by resampling each to $N = 1000$ uniformly spaced samples. (3) The 12 resampled cycles were averaged pointwise to compute a noise-reduced mean cycle $\bar{x}(k)$, $k \in \{1, \dots, N\}$. (4) The averaged cycle was split into forward (extension) and backward (retraction) halves. The backward half was reversed and averaged with the forward half, yielding a symmetric reference motion $\tilde{x}(k)$ with total duration $S = 5.08$ s.

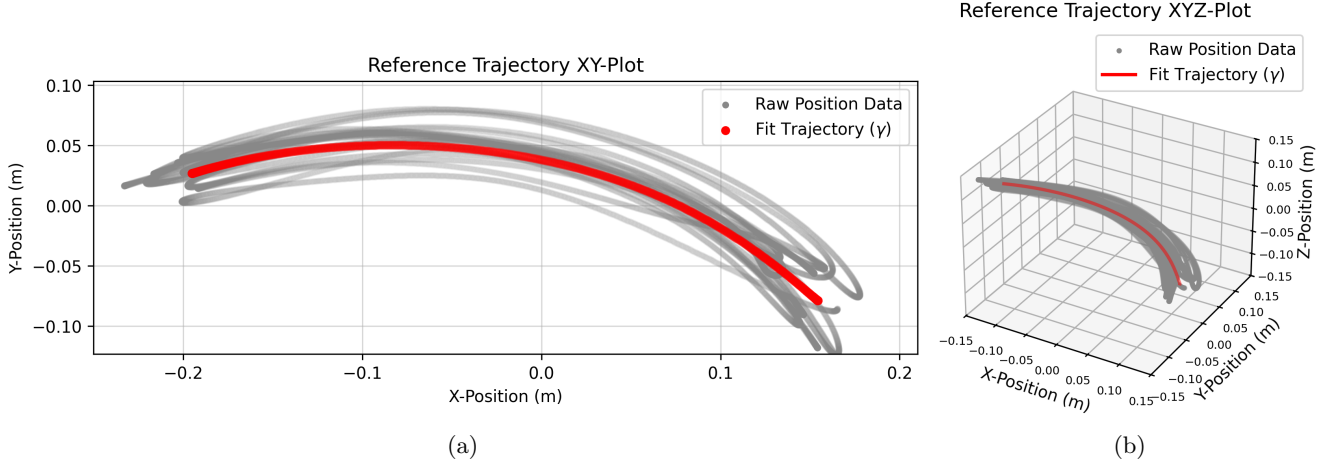


Figure 18: Reference trajectory reconstruction from therapist demonstrations. (a) Projection of 12 therapist-performed shoulder flexion cycles (grey) onto the XY plane, aligned and averaged to produce a smooth reference trajectory (red). (b) 3D visualization of the same trajectory in XYZ space, highlighting the spatial consistency of the therapist’s demonstrations. A cubic spline $\gamma(s)$ was fit to the mean trajectory, enabling continuous reference pose and velocity representations $\gamma(s)$ and $\gamma'(s)$ used by the controller during real-time tracking.

A parametric cubic spline γ was fitted to $\tilde{x}(k)$, with derivatives γ' computed analytically. The spline provides continuous pose and velocity representations:

$$\gamma(s) = \begin{bmatrix} \gamma_x(s) \\ \gamma_y(s) \\ \gamma_z(s) \end{bmatrix}, \quad \gamma'(s) = \frac{d\gamma}{ds}, \quad s \in [0, S]. \quad (47)$$

During operation, the end-effector’s current pose $x(t)$ is projected onto $\gamma(s)$ to determine the closest reference state:

$$s^*(t) = \arg \min_s \|x(t) - \gamma(s)\|, \quad (48)$$

yielding

$$x_{\text{ref}}(t) = \gamma(s^*(t)), \quad \dot{x}_{\text{ref}}(t) = \gamma'(s^*(t)). \quad (49)$$

Visualizations of $\gamma(s)$ and $\gamma'(s)$ are given by Figures 18 and 19.

A.2 Fitting of M and B

The virtual inertia M and damping B in the admittance dynamics (2) were identified from the therapist’s demonstration trials under reference trajectory condition. During the reference trajectory trials, the patient remained passive, allowing us to isolate the therapist’s input. With no verbal guidance ($U_v = 0$) and negligible human force ($F_h \approx 0$), the admittance equation simplifies to

$$M\ddot{x} + B\dot{x} = U_p. \quad (50)$$

The therapist performed 12 repetitions of the exercise while a force sensor on the patient’s wrist recorded $\{U_{p,i}\}_{i=1}^N$ at 100 Hz for $N = 13,168$ samples. Prior to the trial, the patient’s wrist mass was measured as

$$M = 2 \text{ kg} \quad (51)$$

using a calibrated load cell. Position data $\{x_i\}_{i=1}^N$ from motion capture was filtered to remove high-frequency noise, then differentiated numerically to obtain the velocity $\{\dot{x}_i\}_{i=1}^N$ and acceleration $\{\ddot{x}_i\}_{i=1}^N$. With M known, we focused on identifying B . Rearranging (50) isolates the damping term:

$$U_p - M\ddot{x} = B\dot{x} \quad (52)$$

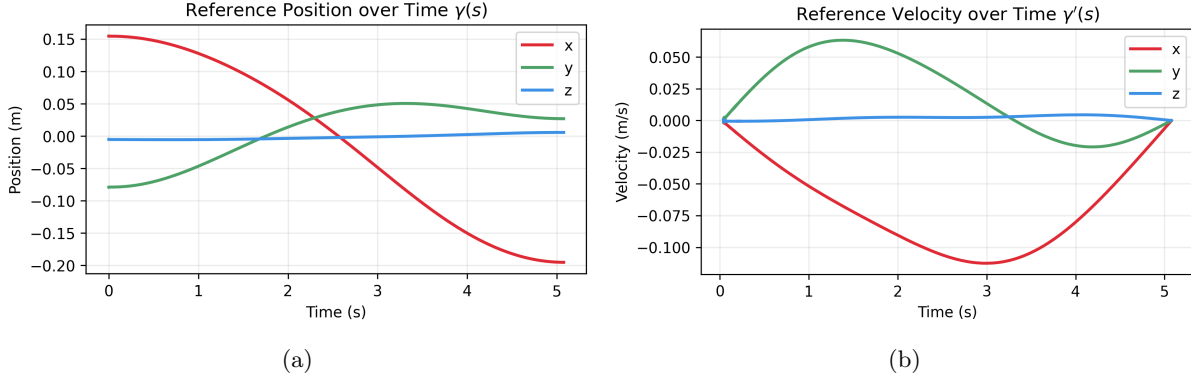


Figure 19: Parametric reference trajectory representations over time. (a) Position components of the fitted cubic spline $\gamma(s)$ along the x , y , and z axes, parameterized over time $s \in [0, S]$. (b) Corresponding velocity components $\gamma'(s)$ computed analytically. The profiles ensure smooth, continuous motion generation for the admittance controller, with dynamics that reflect the temporal asymmetries and spatial couplings observed in the therapist's original demonstrations.

yielding a linear relationship between the dependent variable ($U_p - M\ddot{x}$) and the independent variable (\dot{x}). We used ordinary least squares regression to estimate B :

$$B = \arg \min_B \sum_{i=1}^N \|U_{p,i} - M\ddot{x}_i - B\dot{x}_i\|^2 \quad (53)$$

yielding

$$B = 17.7 \text{ Ns/m} \quad (R^2 = 0.356). \quad (54)$$

A scatter plot of the data and the corresponding fit are given by Figure 20, and a graph comparing the actual force ($U_p - M\ddot{x}$) to the predicted force ($B\dot{x}$) for the reference trajectory trial is given by Figure 21.

A.3 Fitting of K_p, B_p, K_v, B_v

The proportional-derivative (PD) gains K_p, B_p and K_v, B_v were identified from the physical-only and verbal-only trials, respectively.

During the physical-only trial, the therapist applied force corrections without verbal instructions ($U_v = 0$). Assuming negligible verbal compliance effects, the admittance dynamics reduce to:

$$M\ddot{x} + B\dot{x} = K_p e + B_p \dot{e}, \quad (55)$$

where $e = x_{\text{ref}} - x$ and $\dot{e} = \dot{x}_{\text{ref}} - \dot{x}$. Position data $\{x_i\}_{i=1}^N$ from these trials was sampled at 200 Hz for $N = 41224$ samples, with velocity $\{\dot{x}_i\}_{i=1}^N$ and acceleration $\{\ddot{x}_i\}_{i=1}^N$ derived via numerical differentiation. Using the pre-identified M and B given by (51) and (54), ordinary least squares regression was applied to solve:

$$K_p, B_p = \arg \min_{K_p, B_p} \sum_{i=1}^N \|M\ddot{x}_i + B\dot{x}_i - (K_p e_i + B_p \dot{e}_i)\|^2, \quad (56)$$

yielding

$$K_p = 18.8 \text{ N/m}, \quad B_p = 11.4 \text{ Ns/m}, \quad (R^2 = 0.371). \quad (57)$$

Model validation is shown in Figure 23.

For the verbal-only trial, the therapist provided instructions without physical contact ($U_p = 0$). Under the assumption that verbal guidance induces corrective human forces $F_h \approx K_v e + B_v \dot{e}$, the dynamics become:

$$M\ddot{x} + B\dot{x} = K_v e + B_v \dot{e}. \quad (58)$$

Applying the identical procedure to the verbal-only trial, OLS regression produced

$$K_v = 5.64 \text{ N/m}, \quad B_v = 4.78 \text{ Ns/m}, \quad (R^2 = 0.283). \quad (59)$$

Model validation is shown in Figure 22.

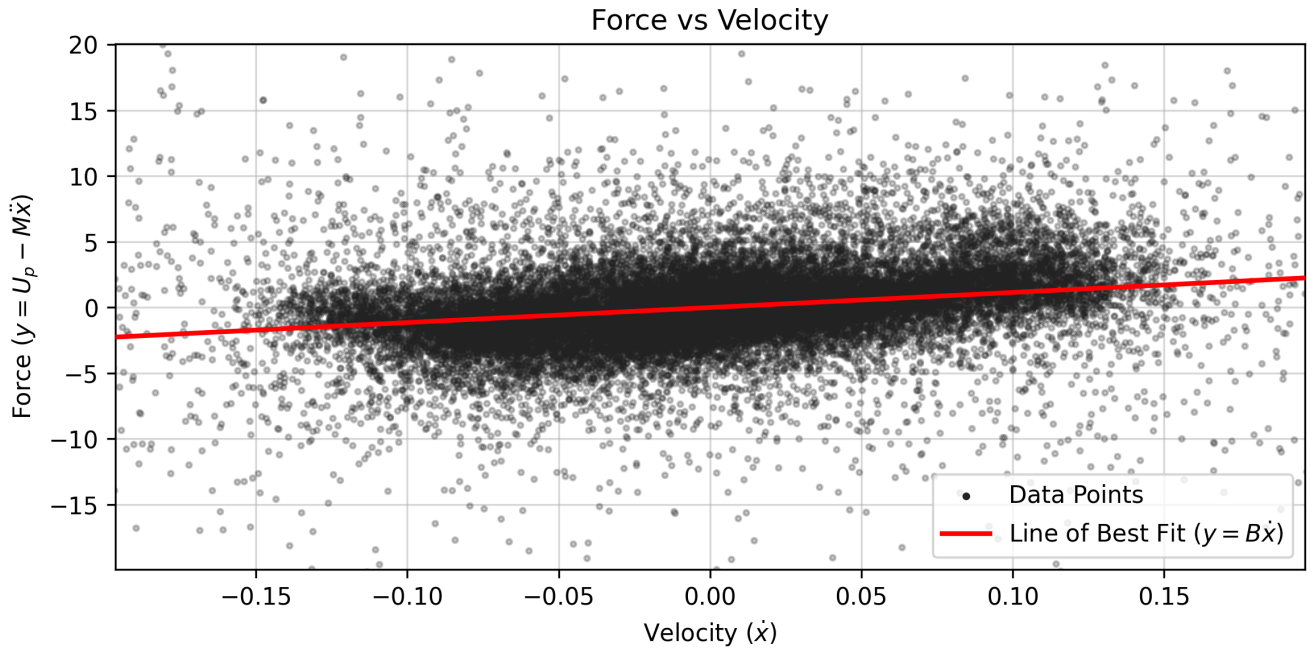


Figure 20: Identification of damping matrix B from therapist demonstration data. Each point corresponds to a sample from the reference trajectory trial, plotting the measured end-effector velocity \dot{x} against the residual force $U_p - M\ddot{x}$. A linear regression (red line) was fit to the data, modeling the damping force as $B\dot{x}$ and yielding the least-squares estimate of $B = 17.7 \text{ Ns/m}$ ($R^2 = 0.356$) used in the admittance controller.

A.4 Transition Probabilities

The compliance transition probabilities $\mathbb{P}(X_t = (i, j) | X_{t-1}, U_{t-1})$ are modeled as time-varying functions of the robot's physical and verbal control inputs U_p and U_v . These probabilities are necessary for the Bayesian filter (Sec. 4.7) to adaptively infer \hat{P}_t and \hat{V}_t . For each prior state $X_{t-1} = (P_{t-1}, V_{t-1})$, transitions to the current state $X_t = (i, j)$ are parameterized by a linear function of the control inputs:

$$\eta_{ij} = a_{ij}||U_p|| + b_{ij}||U_v|| + c_{ij}, \quad (60)$$

where a_{ij}, b_{ij}, c_{ij} are learnable parameters that are unique to each transition pair $(X_{t-1} \rightarrow X_t)$, yielding 16 parameters total. The logits η_{ij} are converted to probabilities via softmax:

$$\mathbb{P}(X_t = (i, j) | X_{t-1}, U_{t-1}) = \frac{\exp(\eta_{ij})}{\sum_{(k,l)} \exp(\eta_{kl})}, \quad (61)$$

which ensures that $\sum_{(i,j)} \mathbb{P}(X_t = (i, j) | X_{t-1}, U_{t-1}) = 1$. The annotated dataset was partitioned into four subsets based on the patient's self-reported prior compliance state X_{t-1} . For each subset, transitions to X_t were labeled as one of four classes: $\{(0,0), (0,1), (1,0), (1,1)\}$. Control inputs $U_{p,t}$ and $U_{v,t}$ were paired with their corresponding $X_{t-1} \rightarrow X_t$ transitions.

Parameters a_{ij}, b_{ij}, c_{ij} for each prior state X_{t-1} were estimated by maximizing the likelihood of the observed compliance state transitions. Equivalently, we minimize the negative log likelihood via cross-entropy loss:

$$\mathcal{L} = - \sum_{(i,j) \in \{0,1\}^2} y_{ij} \log p_{ij}, \quad (62)$$

where $y_{ij} \in \{0,1\}$ indicates the ground-truth transition class, and p_{ij} is the softmax probability given by (61). Optimization was performed using gradient descent. The learned transition probabilities as a function of control inputs are visualized in Figure 24.

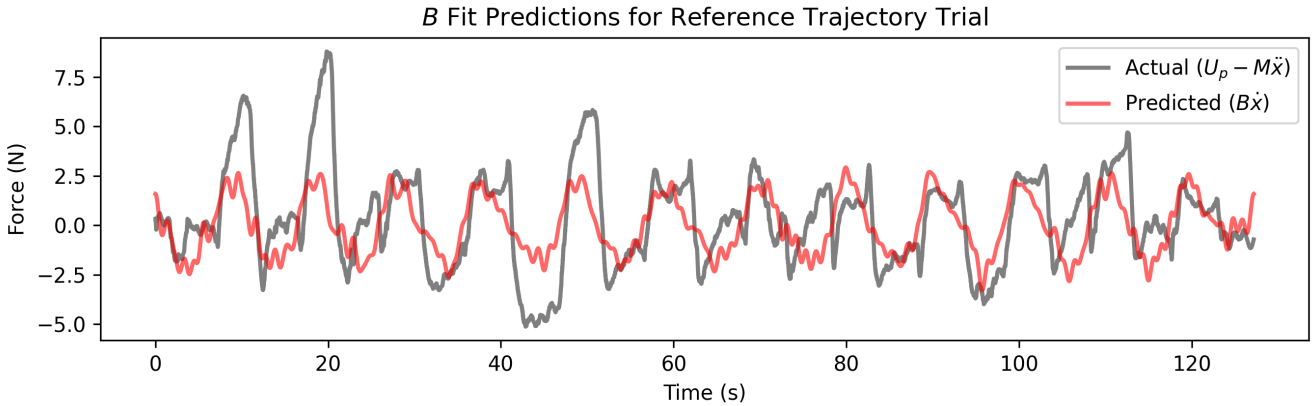


Figure 21: Evaluation of damping model fit over time during the reference trajectory trial. The actual net force $U_p - M\ddot{x}$ (blue) is compared to the predicted damping force $B\dot{x}$ (orange) using the fitted scalar value of $B = 17.7 \text{ Ns/m}$ ($R^2 = 0.356$). Although imperfect, the estimated model captures the dominant temporal trends in damping-related force, validating the use of a linear viscous damping term in our admittance formulation.

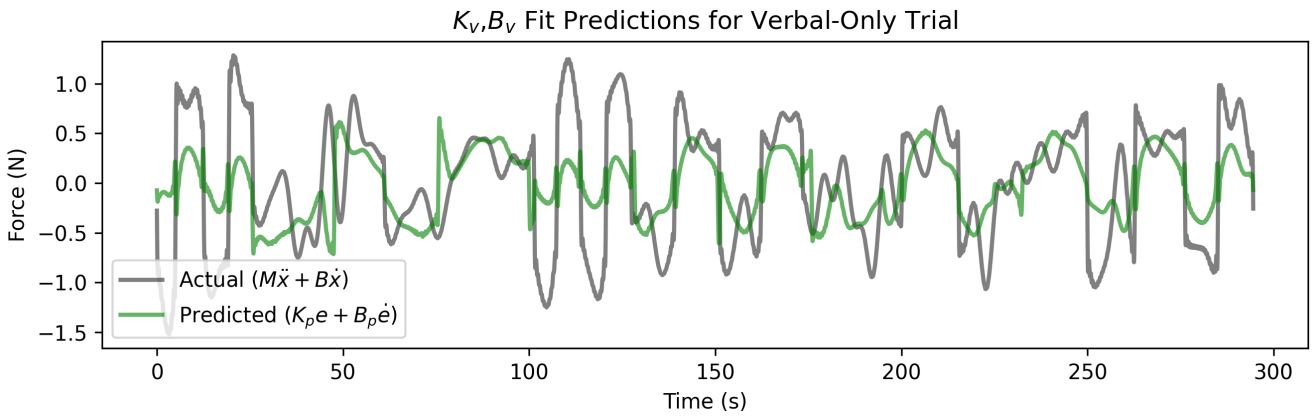


Figure 22: Model fit for verbal control gains K_v , B_v during the verbal-only trial. The measured interaction force $M\ddot{x} + B\dot{x}$ (blue) is compared to the predicted force $K_v e + B_v \dot{e}$ (orange), under the assumption that all correction arose from patient-applied verbal guidance force responses. The model captures the dominant structure in the interaction dynamics, validating the use of a linear PD formulation for verbal guidance.

A.5 Observation PDFs

The observation likelihoods $\mathbb{P}(z_t | X_t = (i, j))$ are modeled as multivariate Gaussian distributions $\mathcal{N}(z_t; \mu_{ij}, \Sigma_{ij})$, where z_t is the tracking error vector, given by (15). The probability density function is defined as:

$$\mathcal{N}(z_t; \mu_{ij}, \Sigma_{ij}) = \frac{1}{\sqrt{(2\pi)^2 |\Sigma_{ij}|}} \exp\left(-\frac{1}{2}(z_t - \mu_{ij})^\top \Sigma_{ij}^{-1} (z_t - \mu_{ij})\right), \quad (63)$$

where μ_{ij} is the mean vector and Σ_{ij} is the positive-definite covariance matrix for state (i, j) .

For each compliance state (i, j) , the dataset was partitioned into subsets $\mathcal{D}_{ij} = \{z_k \mid X_k = (i, j)\}$. The parameters μ_{ij} and Σ_{ij} were computed via maximum likelihood estimation:

$$\mu_{ij} = \frac{1}{N_{ij}} \sum_{z_k \in \mathcal{D}_{ij}} z_k, \quad \Sigma_{ij} = \frac{1}{N_{ij} - 1} \sum_{z_k \in \mathcal{D}_{ij}} (z_k - \mu_{ij})(z_k - \mu_{ij})^\top. \quad (64)$$

The marginal distributions of position and velocity deviations are shown in Figures 25 and 26, while the joint bivariate distributions are visualized in Figure 27.

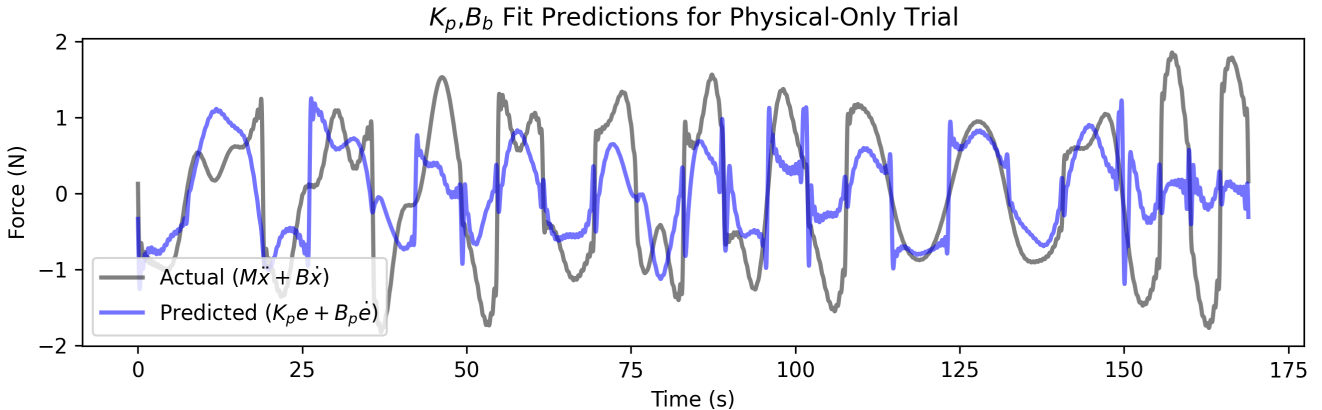


Figure 23: Model fit for physical control gains K_p , B_p during the physical-only trial. The measured interaction force $M\ddot{x} + B\dot{x}$ (blue) is compared to the predicted force $K_p e + B_p \dot{e}$ (orange), under the assumption that all correction arose from therapist-applied physical guidance. The model captures the dominant structure in the interaction dynamics, validating the use of a linear PD formulation for physical guidance.

B Passivity Proof

The derivation of the passivity inequality given by (46) is provided.

Proof of Theorem 1. Recall the storage function $S(t) = \frac{1}{2}\dot{x}^\top M\dot{x} + \frac{1}{2}e^\top K_p e$, where $M \succ 0$ and $K_p \succ 0$. Differentiating with respect to t and using the chain rule gives

$$\dot{S} = \dot{x}^\top M\ddot{x} + e^\top K_p \dot{e}. \quad (65)$$

Invoking the admittance dynamics (2), $M\ddot{x} + B\dot{x} = U_p + F_h$, we have

$$\dot{x}^\top M\ddot{x} = -\dot{x}^\top B\dot{x} + \dot{x}^\top U_p + \dot{x}^\top F_h. \quad (66)$$

Substituting (66) into (65) yields

$$\dot{S} = -\dot{x}^\top B\dot{x} + \dot{x}^\top U_p + \dot{x}^\top F_h + e^\top K_p \dot{e}. \quad (67)$$

Insert the physical control law (45), $U_p = K_p e + B_p \dot{e} - A_p F_h$, into (67):

$$\dot{S} = -\dot{x}^\top B\dot{x} + \dot{x}^\top K_p e + \dot{x}^\top B_p \dot{e} - \dot{x}^\top A_p F_h + \dot{x}^\top F_h + e^\top K_p \dot{e}. \quad (68)$$

Two cross terms contain K_p . Using the error definition (42), $\dot{e} = \dot{x}_{\text{ref}} - \dot{x}$, and the orthogonality property (43), they cancel exactly:

$$\dot{x}^\top K_p e + e^\top K_p \dot{e} = e^\top K_p \dot{x}_{\text{ref}} = 0. \quad (69)$$

The remaining mixed damping term is bounded via the Cauchy–Schwarz inequality:

$$\begin{aligned} \dot{x}^\top B_p \dot{e} &= \dot{x}^\top B_p (\dot{x}_{\text{ref}} - \dot{x}) \\ &\leq -\frac{1}{2}\dot{x}^\top B_p \dot{x} + \frac{1}{2}\dot{x}_{\text{ref}}^\top B_p \dot{x}_{\text{ref}}. \end{aligned} \quad (70)$$

Applying (69) and (70) to (68) produces

$$\dot{S} \leq -\dot{x}^\top (B + \frac{1}{2}B_p) \dot{x} + \frac{1}{2}\dot{x}_{\text{ref}}^\top B_p \dot{x}_{\text{ref}} + \dot{x}^\top (I - A_p) F_h. \quad (71)$$

Because $0 \leq A_p \leq 1$, the last term satisfies $\dot{x}^\top (I - A_p) F_h \leq \dot{x}^\top F_h$. Consequently

$$\dot{S} \leq \dot{x}^\top F_h + \frac{1}{2}\dot{x}_{\text{ref}}^\top B_p \dot{x}_{\text{ref}} - \dot{x}^\top (B + \frac{1}{2}B_p) \dot{x}. \quad (72)$$

The final term in (72) is non-positive because $B + \frac{1}{2}B_p \succ 0$. Integrate (72) from 0 to t :

$$S(t) - S(0) \leq \int_0^t \dot{x}^\top(\tau) F_h(\tau) d\tau + \frac{1}{2} \int_0^t \dot{x}_{\text{ref}}^\top(\tau) B_p \dot{x}_{\text{ref}}(\tau) d\tau. \quad (73)$$

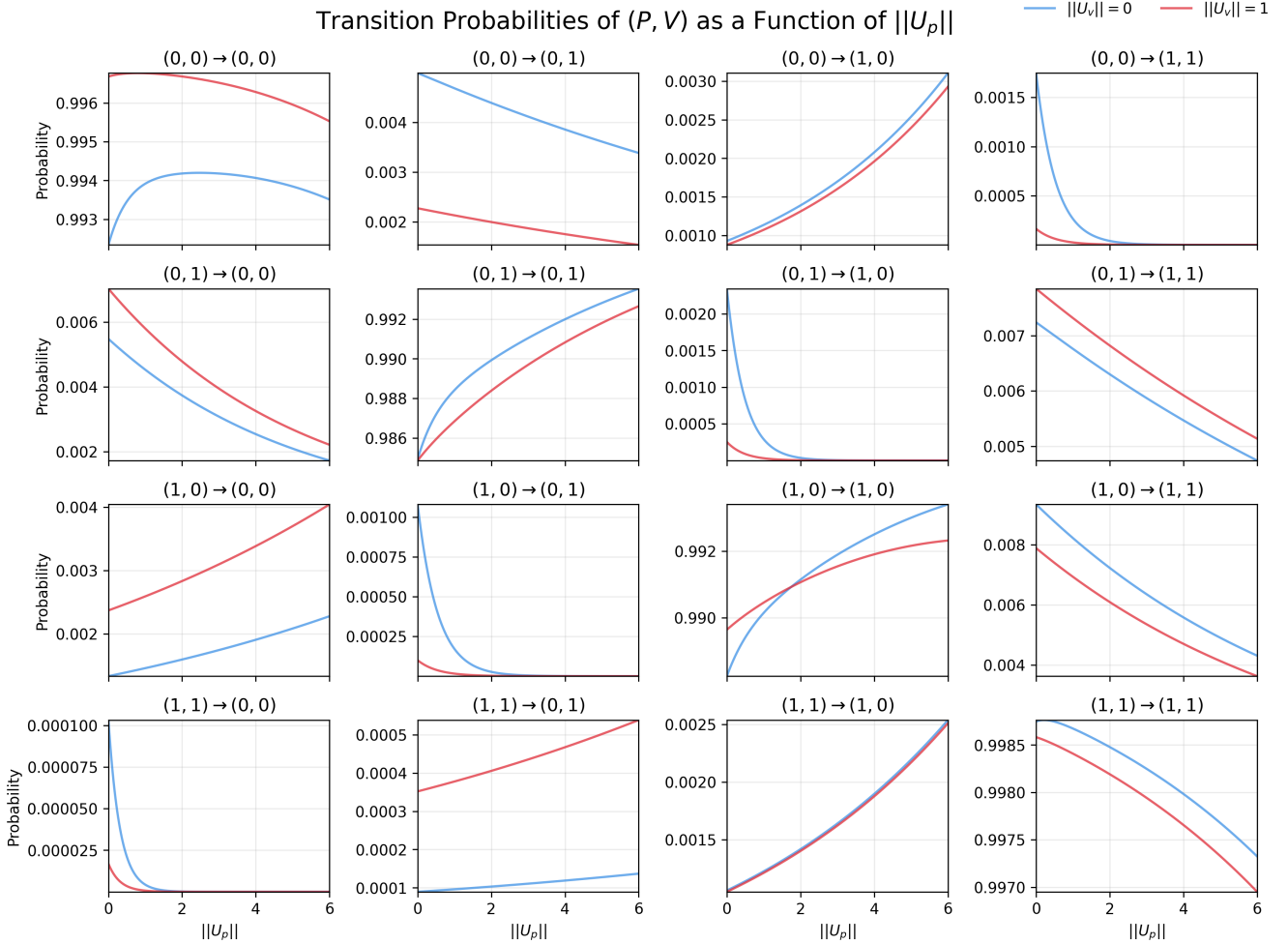


Figure 24: Learned transition probabilities between joint compliance states (P, V) as a function of the physical control magnitude $\|U_p\|$, with separate curves for low and high verbal control magnitudes $\|U_v\| = 0$ (blue) and $\|U_v\| = 1$ (red). Each subplot represents a specific transition pair from prior state (P_{t-1}, V_{t-1}) to current state (P_t, V_t) , showing how the robot’s physical and verbal control efforts influence the likelihood of compliance transitions. These visualizations reflect the learned parameters of the softmax-based transition model (Eq. 61), capturing how higher guidance magnitudes modulate the evolution of compliance.

The reference trajectory is *rest-to-rest* by design (Sec. 4.5); hence $\dot{x}_{\text{ref}}(0) = \dot{x}_{\text{ref}}(t_f) = 0$ and the second integral in (73) is finite for all $t \leq t_f$. Absorbing this finite quantity into the constant $S(0)$ yields precisely the desired inequality (46), i.e.

$$S(t) - S(0) \leq \int_0^t F_h^\top(\tau) \dot{x}(\tau) d\tau, \quad \forall t \in [0, t_f].$$

□

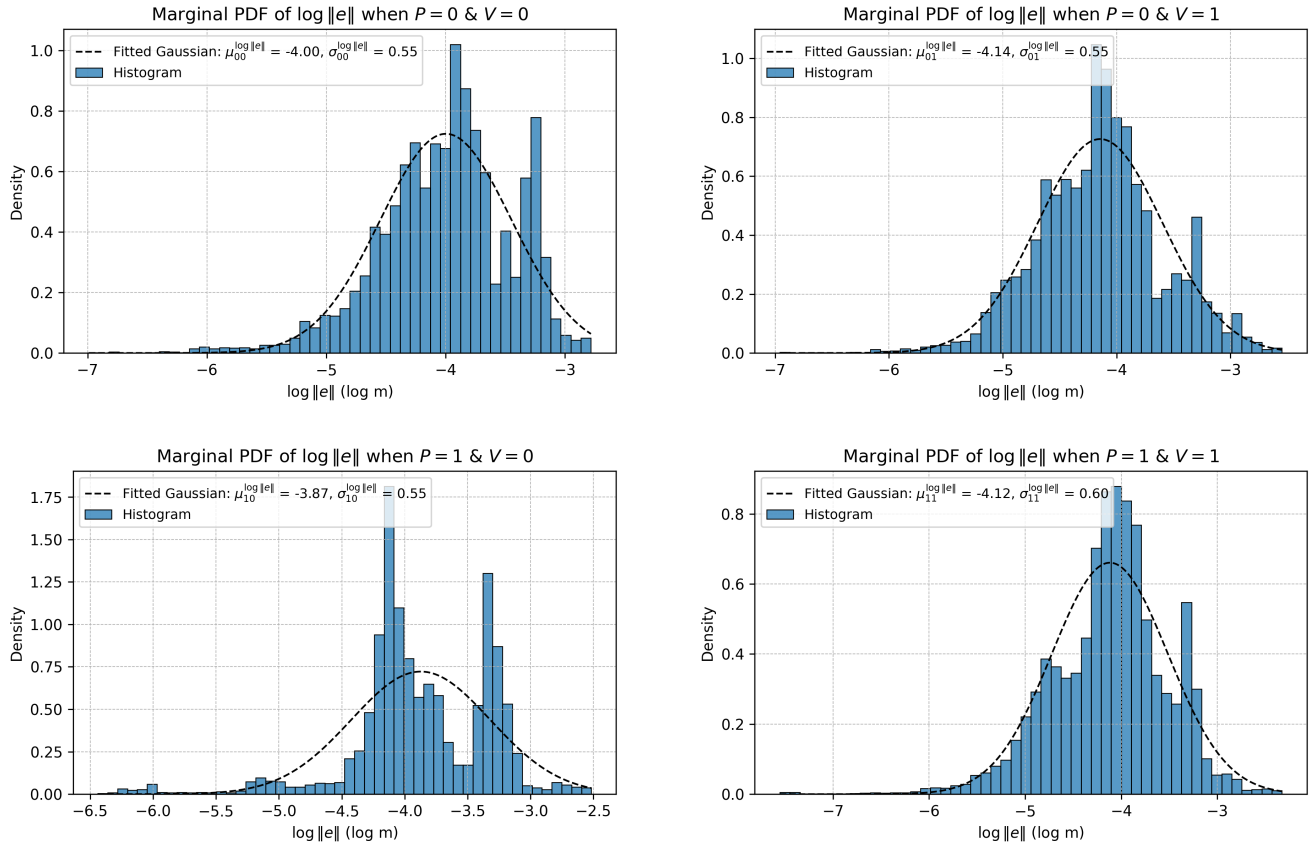


Figure 25: Marginal distributions of log position deviation $\log \|e\|$ for each compliance state $(P, V) \in \{0, 1\}^2$, where $e = x_{\text{ref}} - x$. Each subplot shows a histogram of observed values fit with a multivariate Gaussian estimated via maximum likelihood. Non-compliant states (e.g., $P = 0, V = 0$) exhibit higher means compared to compliant states (e.g., $P = 1, V = 1$), reflecting greater deviation from the reference trajectory—consistent with intuitive expectations of lower adherence under low compliance. These fitted marginals are used to construct the Gaussian observation models $\mathbb{P}(z_t | X_t = (i, j))$.

(a) Compliance Condition: Low Physical, Low Verbal					
Metric	Baseline	Our Method	Obs. Study	$\Delta\%$	p-value
Position Error	0.058 ± 0.016	0.029 ± 0.004	—	$\downarrow 50$	0.0020**
Velocity Error	0.069 ± 0.010	0.057 ± 0.010	—	$\downarrow 17$	0.0038**
Smoothness	0.030 ± 0.005	0.015 ± 0.002	—	$\downarrow 50$	$2.1 \times 10^{-5} ***$
Completion Time (s)	93.67 ± 25.00	68.33 ± 14.26	—	$\downarrow 27$	0.0382*
Median Robot Force (N)	1.762 ± 0.558	1.812 ± 0.313	1.239	—	0.338
Speaking Freq. (w/s)	1.026 ± 0.072	1.292 ± 0.134	1.914	—	0.0042**
Instr./Encour. Ratio	2.309 ± 1.216	1.198 ± 0.311	1.331	—	0.0379*
(b) Compliance Condition: High Physical, Low Verbal					
Metric	Baseline	Our Method	Obs. Study	$\Delta\%$	p-value
Position Error	0.033 ± 0.012	0.017 ± 0.004	—	$\downarrow 48$	0.0092**
Velocity Error	0.039 ± 0.010	0.033 ± 0.008	—	$\downarrow 15$	0.0471*
Smoothness	0.018 ± 0.004	0.011 ± 0.002	—	$\downarrow 39$	0.0105**
Completion Time (s)	68.99 ± 12.32	58.60 ± 12.28	—	$\downarrow 15$	0.139
Median Robot Force (N)	0.788 ± 0.250	0.568 ± 0.222	1.016	—	0.794
Speaking Freq. (w/s)	0.981 ± 0.152	0.868 ± 0.173	0.854	—	0.405
Instr./Encour. Ratio	0.592 ± 0.249	0.962 ± 0.243	1.395	—	0.0252*
(c) Compliance Condition: Low Physical, High Verbal					
Metric	Baseline	Our Method	Obs. Study	$\Delta\%$	p-value
Position Error	0.034 ± 0.009	0.024 ± 0.003	—	$\downarrow 29$	0.0385*
Velocity Error	0.040 ± 0.009	0.037 ± 0.004	—	$\downarrow 8$	0.258
Smoothness	0.020 ± 0.005	0.014 ± 0.002	—	$\downarrow 30$	0.0427*
Completion Time (s)	67.65 ± 15.93	63.19 ± 9.97	—	$\downarrow 7$	0.316
Median Robot Force (N)	0.879 ± 0.229	1.142 ± 0.406	1.149	—	0.853
Speaking Freq. (w/s)	0.883 ± 0.186	0.992 ± 0.143	0.843	—	0.432
Instr./Encour. Ratio	0.672 ± 0.392	1.121 ± 0.526	0.608	—	0.707
(d) Compliance Condition: High Physical, High Verbal					
Metric	Baseline	Our Method	Obs. Study	$\Delta\%$	p-value
Position Error	0.024 ± 0.010	0.021 ± 0.004	—	$\downarrow 13$	0.268
Velocity Error	0.030 ± 0.005	0.028 ± 0.004	—	$\downarrow 7$	0.214
Smoothness	0.013 ± 0.004	0.012 ± 0.002	—	$\downarrow 8$	0.410
Completion Time (s)	45.42 ± 4.21	50.80 ± 7.20	—	$\uparrow 12$	0.898
Normalized Robot Force	0.572 ± 0.172	0.477 ± 0.182	0.596	—	0.536
Speaking Freq. (w/s)	1.109 ± 0.105	0.849 ± 0.156	0.389	—	$9.5 \times 10^{-5} ***$
Instr./Encour. Ratio	0.426 ± 0.181	0.719 ± 0.219	0.665	—	0.198

Table 2: Comparison of our Robot Guidance Controller (Our Method) with the fixed-gain baseline (Baseline) in all four learner-compliance regimes, where $P \in \{0, 1\}$ and $V \in \{0, 1\}$ denote physical and verbal compliance, respectively. Each sub-table reports the mean plus or minus the 95% confidence interval, the percentage change relative to the baseline, and the two-tailed p-value from a paired t-test ($N = 12$ trials per cell). “Obs. Study” lists the value observed in expert therapist-patient demonstrations. Significance markers follow convention: * $p < .05$, ** $p < .01$, *** $p < .001$.

$X_{t-1} \setminus X_t$	$X_t = (0, 0)$	$X_t = (0, 1)$	$X_t = (1, 0)$	$X_t = (1, 1)$
$X_{t-1} = (0, 0)$	0.7180186	0.6531676	0.9194265	-1.1720577
$X_{t-1} = (0, 1)$	0.57513016	0.7693612	-1.3269429	0.69730437
$X_{t-1} = (1, 0)$	0.84166193	-1.0936067	0.7530234	0.6233168
$X_{t-1} = (1, 1)$	-2.9374218	0.3163404	0.39094663	0.24521251

Table 3: Learned a_{ij} values for each transition pair.

$X_{t-1} \setminus X_t$	$X_t = (0, 0)$	$X_t = (0, 1)$	$X_t = (1, 0)$	$X_t = (1, 1)$
$X_{t-1} = (0, 0)$	0.48214963	-0.30785474	0.42163002	-1.8944792
$X_{t-1} = (0, 1)$	0.63350487	0.3842422	-1.8434653	0.4650253
$X_{t-1} = (1, 0)$	1.0996757	-1.8577393	0.5245419	0.35390452
$X_{t-1} = (1, 1)$	-2.3862197	0.7957043	-0.58402497	-0.57316595

Table 4: Learned b_{ij} values for each transition pair.

$X_{t-1} \setminus X_t$	$X_t = (0, 0)$	$X_t = (0, 1)$	$X_t = (1, 0)$	$X_t = (1, 1)$
$X_{t-1} = (0, 0)$	3.3336012	-1.9594908	-3.6424782	-3.0082774
$X_{t-1} = (0, 1)$	-2.864783	2.3264263	-3.714479	-2.5864382
$X_{t-1} = (1, 0)$	-3.484102	-3.6938949	3.1255682	-1.5355915
$X_{t-1} = (1, 1)$	-4.482538	-4.6248226	-2.1531882	4.6947365

Table 5: Learned c_{ij} values for each transition pair

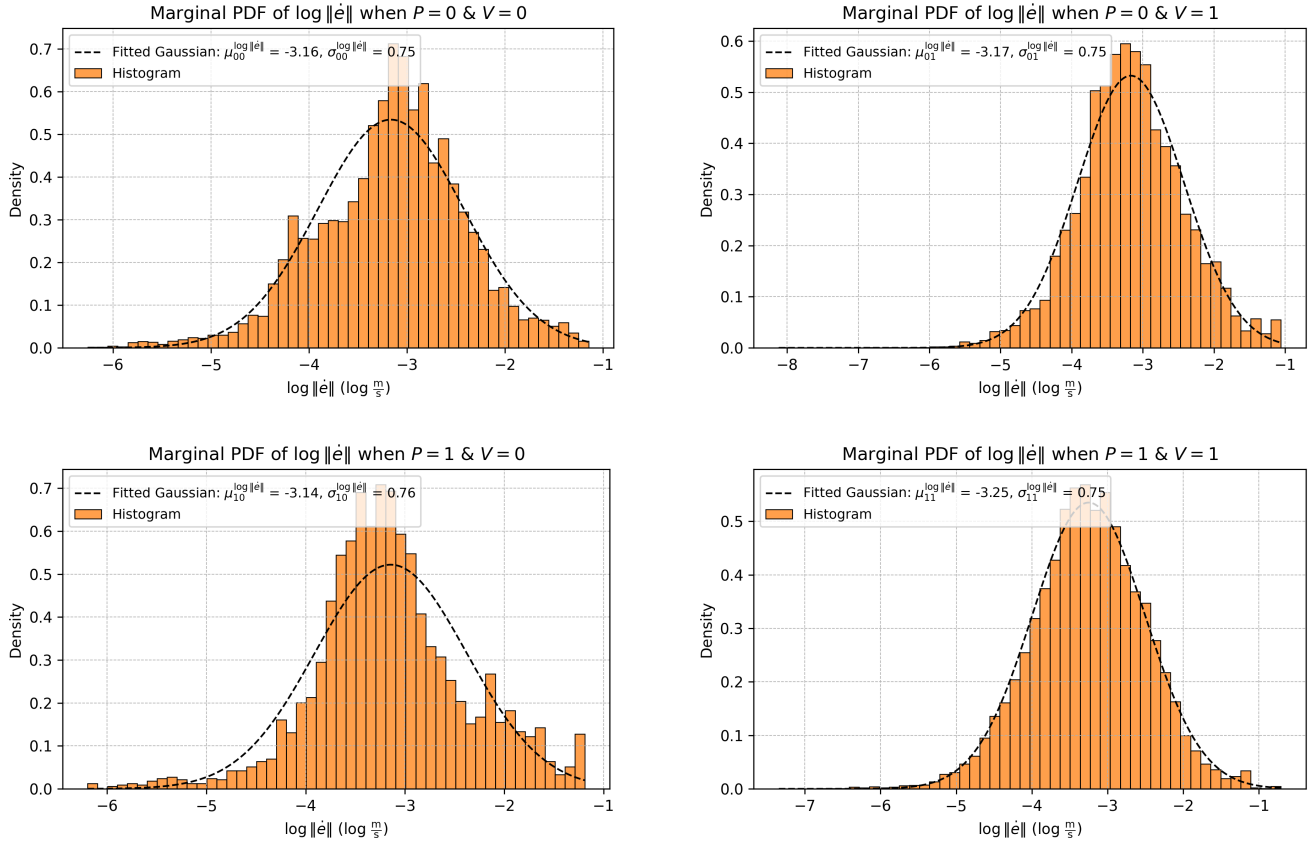


Figure 26: Marginal distributions of log velocity deviation $\log \|\dot{\epsilon}\|$ across all compliance states $(P, V) \in \{0, 1\}^2$, where $\dot{\epsilon} = \dot{x}_{\text{ref}} - \dot{x}$. Each histogram is overlaid with a maximum likelihood Gaussian fit. Similar to position deviations, non-compliant states tend to show higher means, indicating greater difficulty in matching the desired motion. These distributions inform the state-conditioned likelihoods used in the observation model for the Bayesian compliance estimator.

Fitted 2D Gaussian PDF Contours Across Compliance States

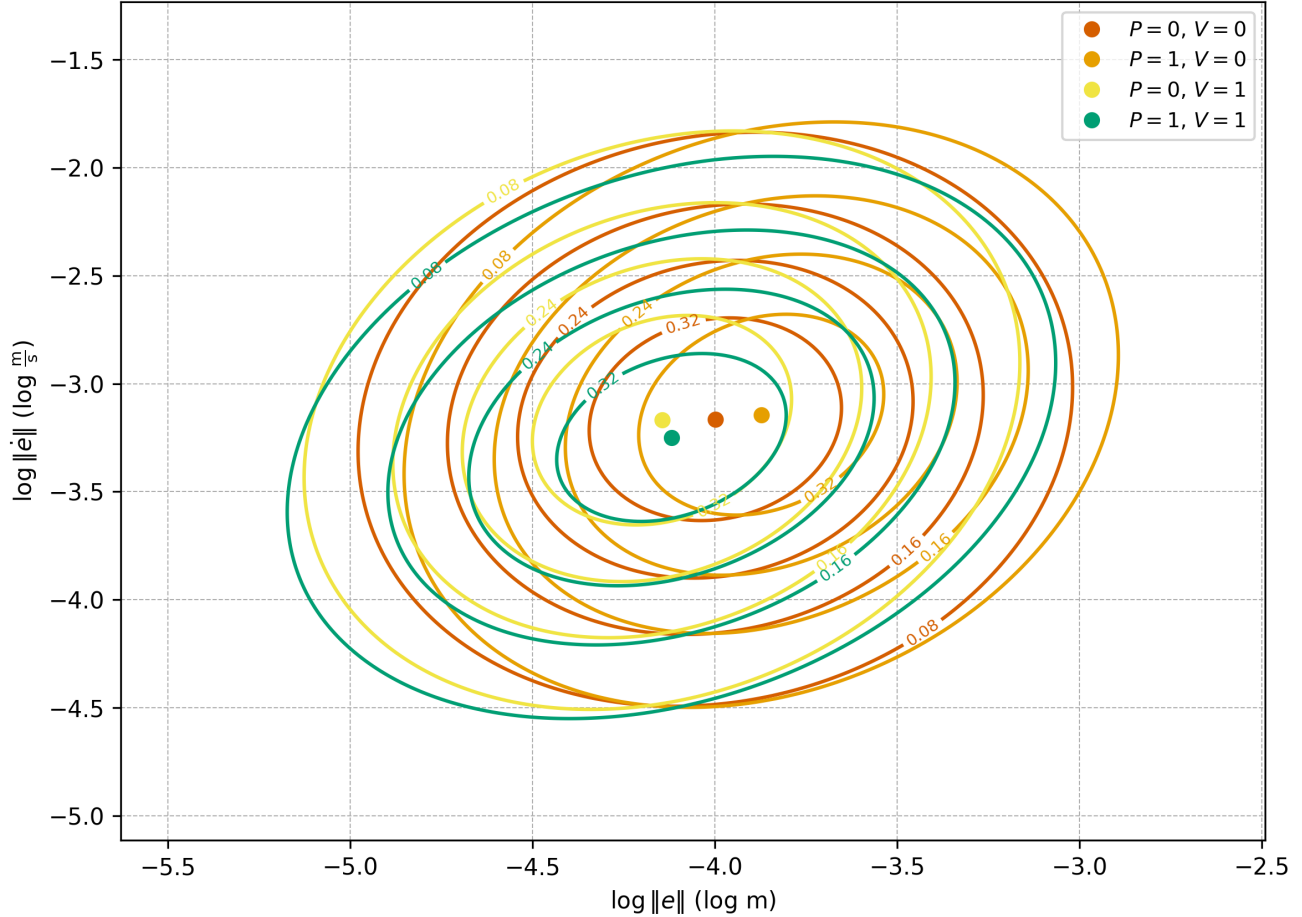


Figure 27: Fitted bivariate Gaussian contours over the joint distribution of $\log \|e\|$ and $\log \|\dot{e}\|$ across all compliance states $(P, V) \in \{0, 1\}^2$. Each contour represents the estimated probability density for a specific state, with ellipses derived from the corresponding mean μ_{ij} and covariance Σ_{ij} computed via maximum likelihood. Non-compliant states (e.g., $P = 0, V = 0$) are shifted toward higher deviation magnitudes, as reflected by their contour centers and spread, while fully compliant states ($P = 1, V = 1$) exhibit lower deviation—supporting the intuition that task compliance correlates with reduced deviation.